nature geoscience

Article

https://doi.org/10.1038/s41561-024-01614-y

# Substantial and overlooked greenhouse gas emissions from deep Arctic lake sediment

Received: 16 March 2024

Accepted: 20 November 2024

Published online: 3 January 2025

Check for updates

Nancy L. Freitas[1,2] ✉, Katey Walter Anthony[3], Josefine Lenz[4], Rachel C. Porras[2] & Margaret S. Torn[1,2] ✉

Thermokarst lakes cause abrupt and sustained permafrost degradation and have the potential to release large quantities of ancient carbon to the atmosphere. Despite concerns about how lakes will affect the permafrost carbon feedback, the magnitude of carbon dioxide and methane emissions from deep permafrost soils remains poorly understood. Here we incubated a very deep sediment core (20 m) to constrain the potential productivity of thawed Yedoma and underlying Quaternary sand and gravel deposits. Through radiocarbon dating, sediment incubations and sediment facies classifications, we show that extensive permafrost thaw can occur beneath lakes on timescales of decades to centuries. Although it has been assumed that shallow, aerobic carbon dioxide production will dominate the climate impact of permafrost thaw, we found that anaerobic carbon dioxide and methane production from deep sediments was commensurate with aerobic production on a per gram carbon basis, and had double the global warming potential at warmer temperatures. Carbon release from deep Arctic sediments may thus have a more substantial impact on a changing climate than currently anticipated. These environments are presently overlooked in estimates of the permafrost carbon feedback.

The northern circumpolar permafrost zone contains approximately one-third of global soil organic carbon (SOC; ~1,100–1,500 Pg C)[1,2]. Over the past 40 years, the Arctic has warmed at four times the global average rate[3], threatening the stability of this carbon. Permafrost thaw exposes organic matter to microbial degradation, which leads to carbon mineralization and release to the atmosphere as carbon dioxide ($CO_2$) and methane ($CH_4$)[4,5]. Some studies suggest that ~5–15% of the known permafrost soil carbon pool (mean 10% value of ~146–160 Pg C) could be lost as greenhouse gas (GHG) emissions by 2100[1,6]. However, these estimates largely focus on surface permafrost (0–3 m), and overlook the size and vulnerability of deeper carbon pools (below 3 m)[2]. One study loosely calculated that permafrost regions might contain as much as 9,000 Pg C if 100+ m of sediment depth was accounted for at 0.5% SOC[7]. Additionally, most estimates of GHG emissions only consider gradual thaw of surface permafrost, and do not account for rapid and much deeper thaw processes that may amplify the permafrost carbon feedback (PCF)[8].

Thermokarst lake formation is a driver of abrupt permafrost degradation and sustained thaw over time[9,10]. As ice-rich permafrost thaws, surface subsidence and pooling water can form lakes that transfer heat into the ground through expansion of an unfrozen talik (thaw bulb)[11]. This can cause very deep sediments[12] to thaw decades faster than active layer deepening[13] and can expose ancient, buried organic matter to microbial decomposition[14–16]. Modelling of lake formation and expansion shows that when thermokarst lakes are included in estimates of the PCF, they could double end-of-century permafrost carbon emissions and increase associated radiative forcing effects by 130% (representative concentration pathway 8.5)[17]. Pleistocene-aged Yedoma is particularly vulnerable to the formation of high GHG-producing lakes due to its ice richness, depths of 50+ m and carbon content[18–20]. Less is

[1]Energy and Resources Group, University of California Berkeley, Berkeley, CA, USA. [2]Climate and Ecosystem Sciences Division, Lawrence Berkeley National Lab, Berkeley, CA, USA. [3]Water and Environmental Research Center, University of Alaska Fairbanks, Fairbanks, AK, USA. [4]Alfred Wegener Institute – Helmholtz Centre for Polar and Marine Research, Permafrost Research Section, Potsdam, Germany. ✉e-mail: nfreitas@berkeley.edu; mstorn@lbl.gov

https://doi.org/10.1038/s41561-024-01614-y

**Table 1 | Incubation sample depth ranges, sediment descriptions, and associated $^{14}$C-dated materials and ages**

| Sample depth range (m) | Sediment description | $^{14}$C material depth (m)[a] | $^{14}$C material description | $^{14}$C age (±2 s.d.) (yr BP) | $^{14}$C calibrated, rounded age (±2 s.d.) (cal yr BP) |
|---|---|---|---|---|---|
| 0.31–0.47 | Minerogenic silt; poorly decomposed organics | 0.50–0.51 | *Sphagnum* | 719 (50) | 680 (50) |
| 0.60–0.76 | Poorly decomposed brown peat (moss and sedge) at top; layered, fine-grained minerogenic sediment with poorly decomposed organic layers (moss) at bottom | 0.88–0.89 | Moss and seeds | 905 (55) | 830 (100) |
| 1.10–1.17 | Moderately decomposed peat with well-preserved wooden remains | 1.10–1.11 | Wood—with bark, needles, moss— stems with leaves, leaf | 980 (50) | 880 (100) |
| | | 1.16–1.17 | Needles, mosses—stems with leaves, seed, leaves | 1,021 (50) | 950 (60) |
| 3.05–3.21 | Dark, minerogenic-dominated sediment with some layered to marbled structures; no visible organics | N/A | N/A | N/A | N/A |
| 5.24–5.39[b] | Brown peat layer with silt and coarse organics visible (moss remains) at top; lighter grey silt with no visible organic remains at bottom | 5.25–5.26[b] | Moss—stems with leaves, *Sphagnum* and others, two seeds, grass | 987 (50) | 880 (100) |
| 7.21–7.35 | Homogenous, olive-grey sediment; mostly moist and sticky, although not as fine as it appears; no visible organics | N/A | N/A | N/A | N/A |
| 10.05–10.20 | Minerogenic sediment; silt with intermediate black layers; no visible organics | N/A | N/A | N/A | N/A |
| 12.62–12.77 | Minerogenic-dominated sediment with a distinct light olive layer | N/A | N/A | N/A | N/A |
| 13.65–13.80 | Very homogenous silt; slight layering with brown but still minerogenic sediment; very well decomposed organics | 13.74 | Wood—well degraded | 54,585 (1,130) | N/A |
| 16.63–16.78 | Well-layered brown, coarse-grained sediment with lighter layers of finer grain sediment—may be floodplain sediment; muscovite and organics visible (rootlets, leaves, bark) | 16.65 | Leaf | >39,600 | N/A |
| 18.52–18.67 | Orange-brown gravel/pebbles; partly well-rounded, partly medium-rounded with a wide range of grain size distribution (up to 2 cm long)—definitely fluvial sediment | N/A | N/A | N/A | N/A |
| 19.83–19.98 | Better sorted sand with no visible structure; some organics visible (wooden remains) | 19.78 | Wood—no bark | >54,300 | N/A |
| | | 20.01–20.02 | Wood | 42,894 (570) | 46,200 (1,140) |

Sediments were described prior to core subsampling and $^{14}$C materials were collected in parallel with incubation sediments. For more extensive down-core descriptions and images, see Supplementary Table 1. N/A, not applicable. [a]$^{14}$C materials were dated from depths that approximately corresponded to the incubation sample depth range, and do not match them exactly. [b]This individual sample may represent an integration of the overlying material due to mixing during sampling (see description in Methods).

known about whether taliks render carbon below Yedoma bioavailable, including Quaternary fluvial sand and gravel deposits that are up to 30 m thick[21,22] and exist in ~10% of Alaskan permafrost landscapes[22,23].

Given that the mechanics of carbon release from deep, thawed sediments are uncertain, their potential feedback to climate warming has not been incorporated within Earth system models[1,8,24,25]. Using a very deep thermokarst lake sediment core, we thus provide a critical knowledge advance about GHG production in shallow peat and lacustrine silt-rich mud (0–5 m), intermediate thawed Yedoma silt (6–15 m) and deep unconsolidated fluvial sediment (16–20 m). We address three existing gaps in understanding: (1) how the geochemistry of a talik varies along a deep sediment profile; (2) which sediments contribute the highest GHG production; and (3) how microbial $CO_2$ and $CH_4$ production changes across depth, redox and climate warming scenarios.

We conducted 365-day incubations, radiocarbon-dated organic materials and classified depth increments associated with different sediment facies (Methods). Briefly, parallel aerobic and anaerobic incubations were run at three temperature treatments; 12 depths were incubated at 4 °C and five depths were also incubated at 10 °C and 20 °C. Each oxygen–temperature–depth combination was incubated in triplicate. Measured values were used to calculate cumulative GHG production in terms of total carbon, global warming impact ($CO_2$e) and temperature sensitivity ($Q_{10}$).

## Lake age and sediment biogeochemical properties

Our characterization of Goldstream Lake (GSL) sediments and organic materials provides evidence of a sobering trajectory for the formation and expansion of thermokarst lakes. The core confirmed earlier geophysical measurements that sediment below GSL was completely thawed to deeper than 20 m (ref. 26). The 1 m depth basal trash layer (the former forest floor[26]) had a $^{14}$C age of 880 ± 100 years (mean ± s.d.; Table 1), indicating that the original lake basin was hundreds of years older than previously estimated by extrapolating lake margin expansion rates without coring[27]. These field-based findings support numerical modelling showing that taliks can thaw thick sequences of permafrost sediments on decade to century timescales, and that thaw can continue for millenia[9,28–30].

Since its inception, inputs of terrestrial organic materials have accumulated in shallow GSL sediments through active thermokarst erosion, deposition and burial processes. These carbon-rich depths are exposed to warmer temperatures with larger seasonal

https://doi.org/10.1038/s41561-024-01614-y

**Table 2 | Incubation sample depth ranges, associated sediment characteristics and treatments (temperature and headspace)**

| | | | | | | | Replicate bottles per temperature treatment (*n*) | |
|---|---|---|---|---|---|---|---|---|
| Sample depth range (m) | Bulk density (g cm$^{-3}$) | Gravimetric water content (%) | Total C (% wt) | Total $C_{org}$ (% wt) | Total N (% wt) | Temperature treatment (°C) | Aerobic | Anaerobic |
| 0.31–0.47 | 1.11 (0.23) | 46.1 | 1.35 (0.54) | 1.04 (0.55) | <0.10 (0.00) | 4, 10, 20 | 3, 3, 3 | 3, 3, 3 |
| 0.60–0.76 | 0.08 (0.03) | 832 | 41.39 (5.87) | 39.57 (6.01) | 1.10 (0.59) | 4 | 3 | 3 |
| 1.10–1.17 | 0.19 (0.10) | 129 | 31.87 (11.44) | 30.70 (11.21) | 1.24 (0.47) | 4 | 3 | 3 |
| 3.05–3.21 | 1.38 (0.03) | 30.3 | 1.96 (0.26) | 1.83 (0.27) | <0.10 (0.00) | 4 | 3 | 3 |
| 5.24–5.39 | 1.21 | 28.5 | 3.67 | 3.86 | <0.10 | 4, 10, 20 | 3, 3, 3 | 3, 3, 3 |
| 7.21–7.35 | 1.60 | 21.2 | 0.56 | <0.10 | <0.10 | 4 | 3 | 3 |
| 10.05–10.20 | 1.48 (0.06) | 23.0 | 1.26 (0.09) | 0.89 (0.06) | <0.10 (0.00) | 4, 10, 20 | 3, 3, 3 | 3, 3, 3 |
| 12.62–12.77 | 1.49 | 26.4 | 1.00 | 0.81 | <0.10 | 4 | 3 | 3 |
| 13.65–13.80 | 1.33 (0.23) | 33.7 | 2.10 (1.24) | 1.94 (1.25) | 0.11 (0.01) | 4 | 3 | 3 |
| 16.63–16.78 | 1.12 (0.01) | 43.2 | 3.14 (0.09) | 3.07 (0.09) | 0.16 (0.00) | 4 | 3 | 3 |
| 18.52–18.67 | 1.34 (0.09) | 5.70 | 0.16 (0.00) | <0.10 (0.00) | <0.10 (0.00) | 4, 10, 20 | 3, 3, 3 | 3, 3, 3 |
| 19.83–19.98 | 1.18 (0.06) | 39.5 | 2.55 (0.35) | 2.59 (0.28) | 0.14 (0.02) | 4, 10, 20 | 3, 3, 3 | 3, 3, 3 |

The s.d. is reported in parentheses. Note that sediment was subsampled from the cores in parallel for both the incubations (associated columns: sample depth range, gravimetric water content, and temperature and headspace treatments) and analysis of sediment characteristics (all additional columns). Based on the amount of available sediment, some depths had a higher sampling frequency for sediment characteristic analyses than others. Where a single value is reported without an s.d., $n=1$; where s.d. is reported in parentheses, $n=2$ or $n=3$.

fluctuations[31,32], conditions that promote faster carbon turnover times than deeper layers[33,34]. In contrast, the underlying intermediate depth, which consisted of taberite (Yedoma that thawed in situ beneath the lake)[35,36], had lower average carbon content than both the shallow sediments and deep Quaternary deposits (Tables 1 and 2). The deep layer contained fluvial coarse-grained sediment (16 m), gravel (18 m) and sand (19 m), which were consistent with descriptions and depths of early-to-middle Pleistocene-aged Fox Gravel deposits in the central Alaska region[21,22]. Notably, while the 18 m depth had low total organic carbon (TOC; <0.10%), the 16 m and 19 m depths contained 2–3% TOC. GSL deep sediment carbon content was thus on par with shallow minerogenic silt, a finding that parallels other deep core geochemical analyses[37].

The temperature of in situ sediment at 20 m was near-freezing (1.45 °C); nonetheless, carbon-mineralizing microbial communities were active throughout the core. Specifically, $CO_2$ production was immediately observed in aerobic and anaerobic incubations at all depths and temperatures. Anaerobic $CH_4$ production lagged by ~50–100 days, but $CH_4$ was also emitted at every depth and temperature during the incubations, and was still increasing for the deepest depths and warmest temperatures on the final day. Previous studies of intact permafrost have shown much longer lag times for $CH_4$ production due to the need for methanogenic community establishment (mean 635 ± 620 days)[38]. Although establishment times in GSL after initial permafrost thaw are unknown, we show that these very deep and cold sediments provide suitable conditions for methanogenic activation and sustained growth.

## Aerobic and anaerobic production potentials

Our results challenge the paradigm in permafrost research that shallow aerobic environments are of greatest importance for GHG production[6,39]. Constraining carbon production under variable oxygen conditions is critical for discerning how changing permafrost hydrology could affect climate feedbacks[40]. We report aerobic and anaerobic production as normalized per gram sediment dry weight to provide a coarse estimate of the absolute quantity of GHG released by soil type, but focus our discussion on production per gram SOC as it indicates the quantity of GHG released relative to the carbon degradability and microbial utilization of organic matter within each soil type. Results are presented first by temperature treatment and second by depth.

When production was summed across the length of the core for all temperature treatments, a greater quantity of total GHG carbon was produced per gram dry weight (gdw) in aerobic environments than anaerobic after 1 year (~6,634 versus ~3,988 ug C gdw$^{-1}$; Extended Data Table 1). These results differed greatly within temperature treatments: anaerobic environments produced 51% that of aerobic at 4 °C, but 92% at 10 °C and 72% at 20 °C. However, when production was normalized by initial quantity of SOC, equivalent amounts of carbon were mineralized in aerobic and anaerobic environments after 1 year (~639 versus ~634 mg C g$^{-1}$ SOC, respectively; Extended Data Table 2). Aerobic production exceeded that of anaerobic by ~27% at 4 °C (~361 versus ~285 mg C g$^{-1}$ SOC, respectively; Fig. 1a,b), but anaerobic production considerably outpaced aerobic production at higher temperatures—this was mainly due to greater $CO_2$ emissions: ~52% more carbon was produced at 10 °C and ~9% more at 20 °C. $CH_4$ production was also highly temperature sensitive and made up ~3.5% of total anaerobic carbon released at 10 °C, and 8.4% at 20 °C. When production ratios were compared across depths for all temperature treatments, shallow sediments released 1.43–2.84 times more carbon aerobically than anaerobically (Extended Data Table 2). While this finding supports existing research showing that aerobic production exceeds anaerobic, our ratios were much lower than previously reported (mean value 3.4)[38,39]. Furthermore, this trend reversed with depth. Production ratios dropped to 1.24–1.76 in intermediate sediments and 0.44–1.45 in deep sediments, where anaerobic production matched or outpaced aerobic production.

Total GHG carbon production also increased with depth under both aerobic and anaerobic conditions. Intermediate and deep sediments largely produced more carbon at a given temperature than shallow sediments, when normalized by gram sediment dry weight (Extended Data Table 1) and gram SOC (Fig. 1a–d and Extended Data Table 2). By the end of the incubations, intermediate and deep sediments had also respired an order of magnitude more of the initial SOC than shallow sediments under aerobic and anaerobic conditions (Extended Data Table 3). The 7 m Yedoma and 18 m fluvial deposits had particularly high carbon mineralization and respired ~5–10 times more of the initial SOC than surrounding sediments. Notably, these

https://doi.org/10.1038/s41561-024-01614-y

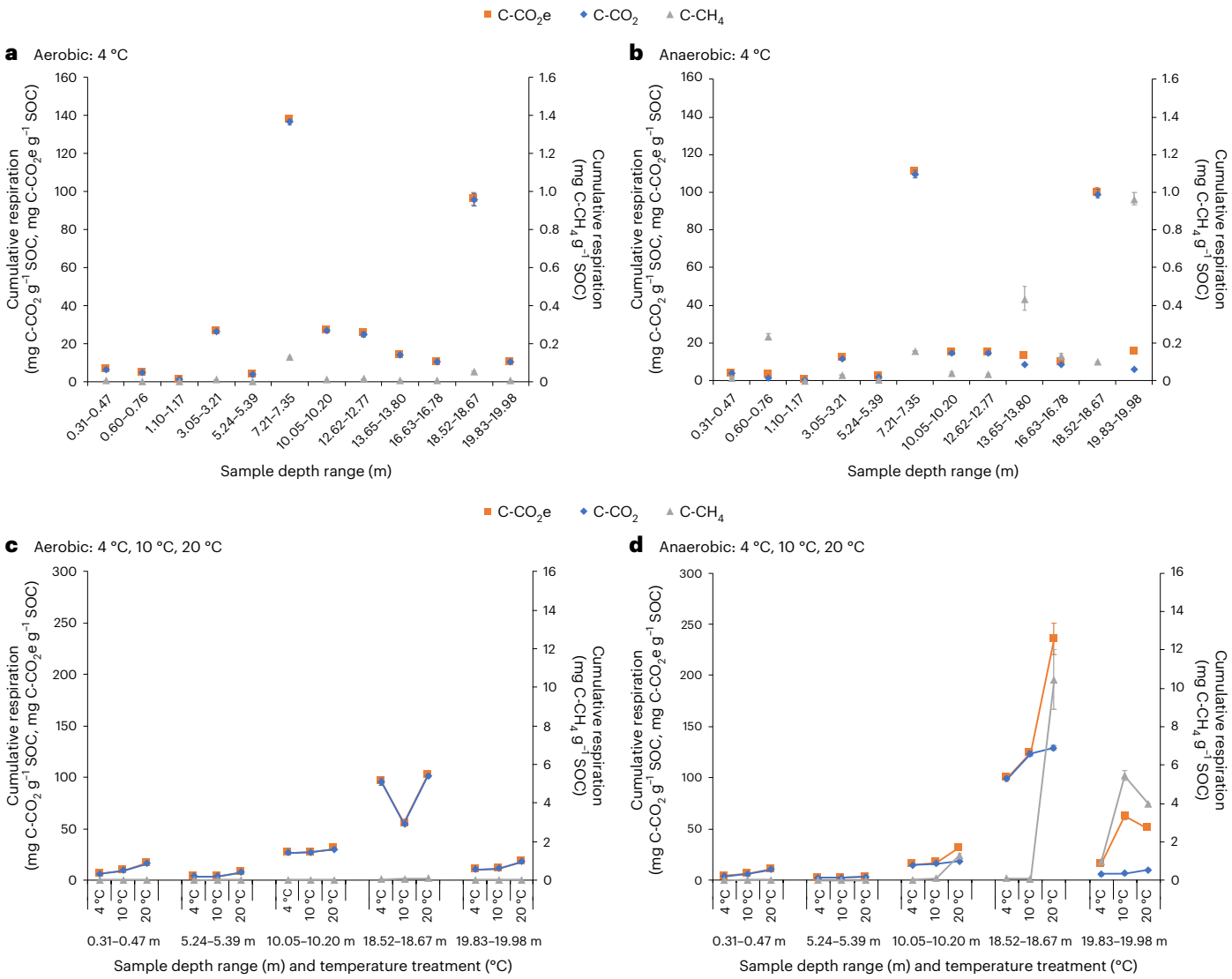


**Fig. 1 | Cumulative C-$CO_2$, cumulative C-$CH_4$ and total C-$CO_2$e produced by day ~365 of the incubations. a**–**d**, Aerobic incubations at 4 °C (**a**), anaerobic incubations at 4 °C (**b**), aerobic incubations at 4 °C, 10 °C and 20 °C (**c**), and anaerobic incubations at 4 °C, 10 °C and 20 °C (**d**). Each value represents an average of the analytical replicates across the final three time points ($n = 9$), normalized by initial quantity of SOC. Error bars show s.e.m. Reference data can be found in Extended Data Table 2.

depths had lower TOC content and higher textural permeability than surrounding sediments (Tables 1 and 2).

Taken together, these patterns may be attributable to: (1) more established anaerobic microbial communities across depth relative to aerobic, because deeper sediments probably have not been exposed to oxic conditions since the Pleistocene; (2) a higher lability of organic matter in intermediate sediments, which was rapidly frozen and preserved during syngenetic Yedoma permafrost formation[18]; (3) microbial access to ancient SOC in deep sediments that was preserved in permafrost for millennia and thawed on more recent timescales; and (4) the possibility that some dissolved organic carbon at 7 m and 18 m was younger than the sediments themselves, and represents surface soil leachates that migrated to coarser-textured sediments with higher hydraulic conductivity[41].

## Global warming potentials and temperature sensitivities

Production was calculated in total carbon equivalents (C-$CO_2$e) to quantify the relative climate impact of potential GHG emissions from different temperatures and sediment depths. This takes into account that $CH_4$ emissions would have a higher global warming potential ($GWP_{100}$ of 28) than $CO_2$ if released to the atmosphere. When summed across temperature treatments, 15% more $CO_2$e was produced anaerobically than aerobically per gram sediment dry weight (~7,681 versus ~6,668 ug C-$CO_2$e $gdw^{-1}$, respectively; Extended Data Table 1), and 32% more per gram SOC (~852 versus ~644 mg C-$CO_2$e $g^{-1}$ SOC; Extended Data Table 2). When differentiated by temperature treatment, total aerobic $CO_2$e production per gram SOC exceeded that of anaerobic by ~19% at 4 °C (Fig. 1a,b). However, at 10 °C and 20 °C, anaerobic $CO_2$e production was twice as high as aerobic (Fig. 1c,d). Similarly high anoxic to oxic production has been found previously, but for intact, terrestrial permafrost incubated at 4 °C (ref. 38). It is possible that greater production of anaerobic $CO_2$e in GSL sediment at high temperatures was due to the temperature sensitivity of methanogenesis and/or that new carbon fractions became available to mineralization that were not exhausted at lower in situ sediment temperatures[31].

$Q_{10}$ coefficients were calculated to determine temperature sensitivity of microbial GHG production (Fig. 2a,b). To disambiguate total $CO_2$e responsiveness, we used a multivariate linear regression to analyse the effects of incubation time and sediment depth on total

https://doi.org/10.1038/s41561-024-01614-y

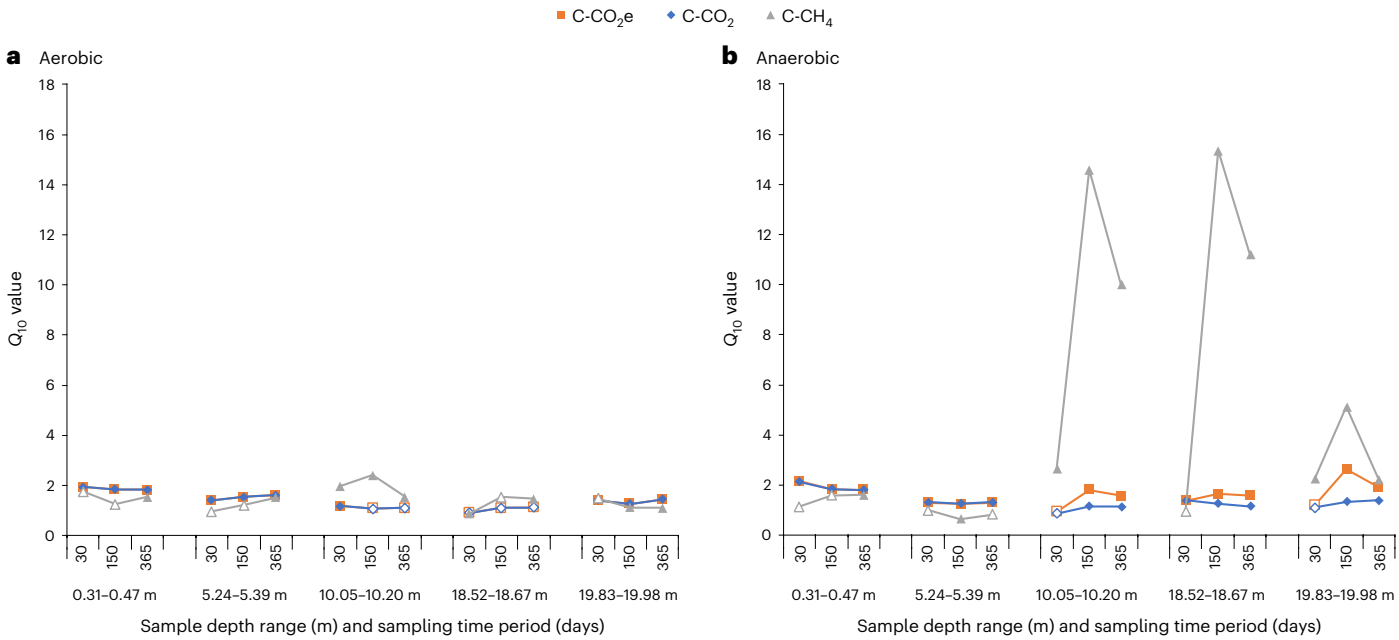


**Fig. 2 | $Q_{10}$ temperature sensitivities by incubation depth at early, middle and end periods of the incubations (30, 150 and 365 days, respectively). a**,**b**, Aerobic incubations (**a**) and anaerobic incubations (**b**). $Q_{10}$ coefficients were computed as a linear regression of cumulative production versus temperature at depths where three incubation temperatures were analysed; data included three time points that bracketed each incubation time period (for example, three time points around the 30-day period), three analytical replicates per time point and three temperatures per time point ($n = 27$). Significant ($P < 0.05$) $Q_{10}$ values are displayed as solid points, whereas insignificant values are open points (insignificance was largely driven by negligible or variable C-$CH_4$ contributions).

C-$CO_2$e, cumulative C-$CO_2$ and cumulative C-$CH_4$ production. In aerobic samples, depth was a significant contributing factor to $CO_2$e production ($P < 0.01$), whereas incubation time was not ($P > 0.10$). In anaerobic samples, neither depth nor incubation time was significant due to steady $CO_2$e production. However, when the overall sensitivity of anaerobic $CO_2$e production was decomposed into constituent $CO_2$ and $CH_4$ sensitivities, anaerobic $CO_2$ $Q_{10}$ values showed significant decreases in responsiveness with depth ($P < 0.05$), whereas $CH_4$ values did not ($P > 0.10$). Together, these results demonstrate that aerobic and anaerobic $CO_2$ temperature sensitivities decreased with depth, but anaerobic depth trends were offset by increasingly sensitive $CH_4$ production.

Owing to high anaerobic $CH_4$ production, aerobic to anaerobic $CO_2$e ratios were considerably lower than those for total GHG carbon production (Extended Data Table 2). In shallow sediments, aerobic production was 1.26–2.17 times that of anaerobic and $CO_2$ made up the majority of $CO_2$e release (except at 0.60 m, 4 °C, where $CH_4$ comprised 62% of $CO_2$e; Extended Data Tables 2 and 3). Intermediate Yedoma sediments had lower production ratios of 0.94–1.72, and $CH_4$ emissions contributed to 42% of the $CO_2$e released at 10 m (20 °C) and 33% at 13 m (4 °C). These ratios became even more striking in the deep unconsolidated deposits, where aerobic to anaerobic production was only 0.18–1.02. Thus, at nearly every deep depth and temperature, anaerobic $CO_2$e emissions matched or exceeded aerobic emissions. $CH_4$ was responsible for up to a staggering 89% of the $CO_2$e produced from deep depths (19 m; Extended Data Table 3). Although minimal $CH_4$ production occurred at 18 m for 4 °C and 10 °C, probably due to low TOC content, very high production was observed at 20 °C for the same depth.

## Sediment column production potentials

We calculated GHG release from the full core to put sediment production potentials into the context of observed emissions at GSL's surface, as well as other Arctic lakes (Methods). Whole sediment column production increased with temperature, and anaerobic production ranged from 64% to 74% that of aerobic, regardless of temperature treatment (Fig. 3 and Extended Data Table 4). This suggests that anaerobic production potentials may be much closer to aerobic than reported within Arctic literature[1,37]. Across the whole sediment column, intermediate Yedoma sediments contributed to the highest amount (~55%) of GHG emissions under both aerobic and anaerobic conditions, but notably, deep unconsolidated sediments contributed the second highest amount (~25%) to anaerobic production (versus shallow sediments in aerobic environments) (Fig. 3 and Extended Data Table 4).

At 4 °C, depth-integrated sediment production potentials in GSL were ~5,484 g C-$CO_2$ $m^{-2}$ $y^{-1}$ under aerobic conditions, and ~3,427 g C-$CO_2$ $m^{-2}$ $y^{-1}$ and ~87 g C-$CH_4$ $m^{-2}$ $y^{-1}$ under anaerobic (Fig. 3 and Extended Data Table 4). Sediment production was therefore only 2.18 (anaerobic) to 3.40 (aerobic) times higher on average than observed emissions at the lake surface (1,583 g C-$CO_2$ $m^{-2}$ $y^{-1}$; 30.3 g C-$CH_4$ $m^{-2}$ $y^{-1}$)[42]. Annual recorded emissions from the surface of GSL are also consistent with those from other Yedoma-type lakes (mean 784 g C-$CO_2$ $m^{-2}$ $y^{-1}$; 44.2 g C-$CH_4$ $m^{-2}$ $y^{-1}$), although they are higher than those from non-Yedoma lakes (mean 137 g C-$CO_2$ $m^{-2}$ $y^{-1}$; 8.0 g C-$CH_4$ $m^{-2}$ $y^{-1}$)[42]. These findings are important for resolving differences between sediment production and consumption potentials versus actual emissions from expanding Yedoma-type lakes.

## Implications of deep sediment GHG production

While newly formed thermokarst lakes are poised to play a pivotal role in carbon mobilization this century[13,16], older lakes with self-sustaining thaw processes[8] may continue emitting GHG over century to millennial timescales. We show that this could be due to a more dynamic deep carbon reservoir than previously understood. Talik development can thaw tens of metres of permafrost below thermokarst lakes within decades to centuries of their formation[28–30,43]. However the decomposition time for labile SOC and associated GHG emission is a function of the rate of talik expansion into underlying sediments, and can continue until expansion slows and carbon-rich layers are depleted over centuries[26] to millennia[9]. We not only demonstrate that 20 m of sediment remained productive at low temperatures beneath an 800+-year-old thermokarst lake, but suggest that previously thawed sediments may initiate new releases of

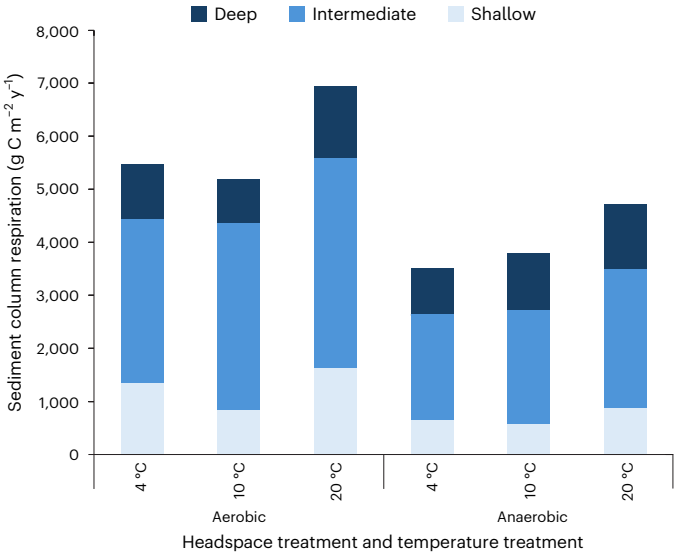


**Fig. 3 | GSL annual sediment column production potentials for total carbon [C-$CO_2$ + C-$CH_4$].** Each bar represents a whole core production potential. Depth-integrated production was calculated for all analytical replicates within a given depth increment, temperature and headspace treatment, across the final three incubation time points ($n$ = variable by depth–temperature combination; see Table 2). Reference data can be found in Extended Data Table 4.

GHG as sediment temperatures rise with climate-driven warming—not simply act as low-level background lake emissions.

In particular, our study provided novel evidence of the high productivity of ancient, unconsolidated fluvial deposits below Yedoma. Given that they are distinct from Yedoma sediments and underlying bedrock, these deposits may require their own designation as a deep carbon pool[2]. Their carbon source may be early-to-mid Pleistocene when streams were active[21] and/or include contributions of younger, more labile dissolved organic carbon from terrestrial ecosystem sources that have been transported into supra-permafrost aquifers[28,41]. If contemporary dissolved organic carbon bypasses near-surface aerobic mineralization and is transported into deep groundwater, then it is more likely to be a feedstock for anaerobic GHG production. This could generate fluxes with greater implications for the PCF on decade to century timescales. The spatial extent of unconsolidated deposits on the landscape, their depth down to tens to hundreds of metres and their high microbial productivity indicates that this could have wide-reaching implications for carbon mobilization as the Arctic thaws[22,23]. These findings call for future research that examines carbon sources, decomposability, turnover times and microbial activity in deep soils.

Although our study was limited to a single deep core from a Yedoma-type thermokarst lake, it lends evidence to a growing body of literature converging around the importance of including deep, anaerobic sediments in estimates of the PCF[17,38]. In a simple extrapolation of sediment productivity to a pan-Arctic scale (Methods), we find that emissions from expanding Yedoma-type thermokarst lakes could be approximately ~0.03–0.09 Pg C $yr^{-1}$. These estimates are probably conservative, as they assume uniform 4 °C sediment temperatures and that 5–15% of annual potential production is released to the atmosphere[1,13]. It is probable that some quantity of these emissions represent a net GHG addition to the atmosphere on top of all permafrost carbon sources (0.5–2.0 Pg C $yr^{-1}$)[44] given that current estimates expect anaerobic emissions will be 78–85% lower than aerobic[1], an assumption actively challenged by this study.

Our results indicate that the climate modelling community may be underestimating the ability for thermokarst lakes to mobilize GHG from intermediate and deep carbon pools. This could have serious consequences for our understanding of current and future Arctic permafrost emissions and their impact on global carbon budgets. To improve estimates of the PCF, our work calls for Earth system models to incorporate: (1) explicit representations of thermokarst ponds and lakes, abrupt and sustained thaw processes, lake expansion and drainage trajectories, carbon pools deeper than 3 m, and sediment types with variable carbon content and decomposability; and (2) spatially and temporally variable mechanisms of GHG release from sediment, such as aerobic and anaerobic conditions, sediment temperatures, and diffusion and ebullition pathways.

## Online content

Any methods, additional references, Nature Portfolio reporting summaries, source data, extended data, supplementary information, acknowledgements, peer review information; details of author contributions and competing interests; and statements of data and code availability are available at https://doi.org/10.1038/s41561-024-01614-y.

## References

1. Schuur, E. A. G. et al. Climate change and the permafrost carbon feedback. *Nature* **520**, 171–179 (2015).
2. Hugelius, G. et al. Estimated stocks of circumpolar permafrost carbon with quantified uncertainty ranges and identified data gaps. *Biogeosciences* **11**, 6573–6593 (2014).
3. Rantanen, M. et al. The Arctic has warmed nearly four times faster than the globe since 1979. *Commun. Earth Environ.* **3**, 168 (2022).
4. Zimov, S. A. et al. North Siberian lakes: a methane source fueled by Pleistocene carbon. *Science* **277**, 800–802 (1997).
5. Schuur, E. A. G. et al. Vulnerability of permafrost carbon to climate change: implications for the global carbon cycle. *BioScience* **58**, 701–714 (2008).
6. Schuur, E. A. G., McGuire, A. D., Romanovsky, V., Schädel, C. & Mack, M. in *Second State of the Carbon Cycle Report* (eds Cavallaro, N. et al.) Ch 11, 428–468 (US Global Change Research Program, 2018); https://doi.org/10.7930/SOCCR2.2018.Ch11
7. Semiletov, I. P. et al. Atmospheric carbon emission from North Asian lakes: a factor of global significance. *Atmos. Environ.* **30**, 1657–1671 (1996).
8. Turetsky, M. R. et al. Carbon release through abrupt permafrost thaw. *Nat. Geosci.* **13**, 138–143 (2020).
9. Kessler, M. A., Plug, L. J. & Walter Anthony, K. M. Simulating the decadal- to millennial-scale dynamics of morphology and sequestered carbon mobilization of two thermokarst lakes in NW Alaska. *J. Geophys. Res. Biogeosci.* https://doi.org/10.1029/2011JG001796 (2012).
10. Zimov, S. A., Schuur, E. A. G. & Chapin, F. S. Permafrost and the global carbon budget. *Science* **312**, 1612–1613 (2006).
11. Grosse, G., Jones, B. & Arp, C. in *Treatise on Geomorphology* Vol. 8 (eds Shroder, J. F. et al.) 325–353 (Academic, 2013); https://doi.org/10.1016/B978-0-12-374739-6.00216-5
12. Johnston, G. H. & Brown, R. J. E. Effect of a lake on distribution of permafrost in the Mackenzie River delta. *Nature* **192**, 251–252 (1961).
13. Schneider von Deimling, T. et al. Observation-based modelling of permafrost carbon fluxes with accounting for deep carbon deposits and thermokarst activity. *Biogeosciences* **12**, 3469–3488 (2015).
14. Elder, C. D. et al. Seasonal sources of whole-lake $CH_4$ and $CO_2$ emissions from interior Alaskan thermokarst lakes. *J. Geophys. Res. Biogeosci.* **124**, 1209–1229 (2019).
15. Langer, M. et al. Rapid degradation of permafrost underneath waterbodies in tundra landscapes—toward a representation of thermokarst in land surface models. *J. Geophys. Res. Earth Surf.* **121**, 2446–2470 (2016).

16. Walter Anthony, K. et al. Methane emissions proportional to permafrost carbon thawed in Arctic lakes since the 1950s. *Nat. Geosci.* **9**, 679–682 (2016).
17. Walter Anthony, K. et al. 21st-century modeled permafrost carbon emissions accelerated by abrupt thaw beneath lakes. *Nat. Commun.* **9**, 3262 (2018).
18. Strauss, J. et al. Deep Yedoma permafrost: a synthesis of depositional characteristics and carbon vulnerability. *Earth-Sci. Rev.* **172**, 75–86 (2017).
19. Kanevskiy, M., Shur, Y., Fortier, D., Jorgenson, M. T. & Stephani, E. Cryostratigraphy of late Pleistocene syngenetic permafrost (Yedoma) in northern Alaska, Itkillik River exposure. *Quat. Res.* **75**, 584–596 (2011).
20. French, H. & Shur, Y. The principles of cryostratigraphy. *Earth-Sci. Rev.* **101**, 190–206 (2010).
21. Hamilton, T. D., Craig, J. L. & Sellmann, P. V. The Fox permafrost tunnel: a Late Quaternary geologic record in central Alaska. *Geol. Soc. Am. Bull.* **100**, 948–969 (1988).
22. Péwé, T. L. *Quaternary Stratigraphic Nomenclature in Unglaciated Central Alaska* Series No. 862 (USGS, 1975).
23. Péwé, T. L. *Quaternary Geology of Alaska* Series No. 835 (USGS, 1975).
24. Koven, C. D. et al. A simplified, data-constrained approach to estimate the permafrost carbon–climate feedback. *Phil. Trans. R. Soc. Math. Phys. Eng. Sci.* **373**, 20140423 (2015).
25. Schaefer, K., Lantuit, H., Romanovsky, V. E., Schuur, E. A. G. & Witt, R. The impact of the permafrost carbon feedback on global climate. *Environ. Res. Lett.* **9**, 085003 (2014).
26. Walter Anthony, K. M. et al. Decadal-scale hotspot methane ebullition within lakes following abrupt permafrost thaw. *Environ. Res. Lett.* **16**, 035010 (2021).
27. Walter Anthony, K. M. & Anthony, P. Constraining spatial variability of methane ebullition seeps in thermokarst lakes using point process models. *J. Geophys. Res. Biogeosci.* **118**, 1015–1034 (2013).
28. Wellman, T. P., Voss, C. I. & Walvoord, M. A. Impacts of climate, lake size, and supra- and sub-permafrost groundwater flow on lake-talik evolution, Yukon Flats, Alaska (USA). *Hydrogeol. J.* **21**, 281–298 (2013).
29. West, J. J. & Plug, L. J. Time-dependent morphology of thaw lakes and taliks in deep and shallow ground ice. *J. Geophys. Res. Earth Surf*. https://doi.org/10.1029/2006JF000696 (2008).
30. Ling, F. & Zhang, T. Numerical simulation of permafrost thermal regime and talik development under shallow thaw lakes on the Alaskan Arctic Coastal Plain. *J. Geophys. Res. Atmos.* https://doi.org/10.1029/2002JD003014 (2003).
31. Heslop, J. K., Walter Anthony, K. M., Grosse, G., Liebner, S. & Winkel, M. Century-scale time since permafrost thaw affects temperature sensitivity of net methane production in thermokarst-lake and talik sediments. *Sci. Total Environ.* **691**, 124–134 (2019).
32. Greene, S., Walter Anthony, K. M., Archer, D., Sepulveda-Jauregui, A. & Martinez-Cruz, K. Modeling the impediment of methane ebullition bubbles by seasonal lake ice. *Biogeosciences* **11**, 6791–6811 (2014).
33. Schädel, C. et al. Circumpolar assessment of permafrost C quality and its vulnerability over time using long-term incubation data. *Glob. Change Biol.* **20**, 641–652 (2014).
34. Gudasz, C., Sobek, S., Bastviken, D., Koehler, B. & Tranvik, L. J. Temperature sensitivity of organic carbon mineralization in contrasting lake sediments. *J. Geophys. Res. Biogeosci.* **120**, 1215–1225 (2015).
35. Walter Anthony, K. M. et al. A shift of thermokarst lakes from carbon sources to sinks during the Holocene epoch. *Nature* **511**, 452–456 (2014).
36. Farquharson, L., Anthony, K. W., Bigelow, N., Edwards, M. & Grosse, G. Facies analysis of Yedoma thermokarst lakes on the northern Seward Peninsula, Alaska. *Sediment. Geol.* **340**, 25–37 (2016).
37. Knoblauch, C., Beer, C., Sosnin, A., Wagner, D. & Pfeiffer, E.-M. Predicting long-term carbon mineralization and trace gas production from thawing permafrost of northeast Siberia. *Glob. Change Biol.* **19**, 1160–1172 (2013).
38. Knoblauch, C., Beer, C., Liebner, S., Grigoriev, M. N. & Pfeiffer, E.-M. Methane production as key to the greenhouse gas budget of thawing permafrost. *Nat. Clim. Change* **8**, 309–312 (2018).
39. Schädel, C. et al. Potential carbon emissions dominated by carbon dioxide from thawed permafrost soils. *Nat. Clim. Change* **6**, 950–953 (2016).
40. Lawrence, D. M., Koven, C. D., Swenson, S. C., Riley, W. J. & Slater, A. G. Permafrost thaw and resulting soil moisture changes regulate projected high-latitude $CO_2$ and $CH_4$ emissions. *Environ. Res. Lett.* **10**, 094011 (2015).
41. Youcha, E. K. *A Geohydrologic Analysis of an Upland-Bedrock Aquifer System: Applications to Interior Alaska*. MSc thesis, Univ. Alaska Fairbanks (2003).
42. Sepulveda-Jauregui, A., Walter Anthony, K. M., Martinez-Cruz, K., Greene, S. & Thalasso, F. Methane and carbon dioxide emissions from 40 lakes along a north–south latitudinal transect in Alaska. *Biogeosciences* **12**, 3197–3223 (2015).
43. Heslop, J. K. et al. Thermokarst lake methanogenesis along a complete talik profile. *Biogeosciences* **12**, 4317–4331 (2015).
44. Schuur, E. A. G. et al. Permafrost and climate change: carbon cycle feedbacks from the warming Arctic. *Annu. Rev. Environ. Resour.* **47**, 343–371 (2022).

# Methods

## Site selection

GSL (64.916° N, 147.847° W) is a thermokarst lake formed in Yedoma permafrost[19] and located in the Goldstream Valley in interior Alaska, ~15 km north of Fairbanks. GSL was selected because it is well studied with respect to $CH_4$ emissions and talik properties[14,26,27,32,45], although very little work has been done on lake sediments[46] and none on deep sediments. The region is characterized by discontinuous permafrost[47,48]. Annual atmospheric temperature and precipitation averages are −2.4 °C and 274 mm, respectively (Fairbanks International Airport, 1981–2010 annual/seasonal normals, US National Climatic Data Center).

GSL (0.010 $km^2$, 4.4 m maximum depth)[26,42] formed from the melting of permafrost ground ice in late Pleistocene Yedoma-type deposits[27]. Pooled water thawed previously frozen Quaternary aeolian deposits both vertically and laterally, enabling thermokarst expansion at depth and along lake margins. A partial drainage event occurred between 1949 and 1978[45], but GSL is still undergoing active thermokarst expansion along its eastern and southern edges[26]. Extensive studies have been conducted on GSL that describe ebullition (bubbling) and diffusive GHG composition, distribution and flux[14,26,27,32,45]. Physical and chemical analyses have also been conducted on the surface water and surface sediments of the lake[49].

## Lake sediment coring

Sediment coring was conducted 16–17 March 2018 in the north-central basin of GSL at a water depth of 1.39 m. All samples were collected (and exported) in a responsible manner and in accordance with relevant permits and local laws. The coring location represented the approximate centre of the lake in 1949. A vibracorer was used to extract surface sediments (down to 4.40 m) in a single core tube (7.5 cm internal diameter; 64.91588° N, 147.84901° W ± 9 ft). In an immediately adjacent coring site (64.91582° N, 147.84935° W ± 9 ft), a Boart Longyear diamond core drilling system was used to extract deep sediments (down to 20.13 m) using percussion drilling. The coring setup consisted of a casing around the borehole that extended up through the lake water and ice to just below the drill rig. A core barrel with an internal plastic liner travelled up and down inside the casing. The casing was not installed at once down to 20 m; it was pushed down incrementally in 3.2 m sections as coring progressed. Continuous core sections were extracted in clear plastic liners (8.9 cm internal diameter) nested in a 1.8-m-long core barrel from within the cased sediments.

No intact permafrost was encountered during coring. We cannot, however, rule out the existence of deeper permafrost because the groundwater that was encountered in the fluvial sediments at the base of the core was not artesian, and groundwater in pressurized, sub-permafrost aquifers is known to be artesian in the vicinity of GSL. To monitor in situ sediment conditions, a pressure transducer and temperature sensor were installed within the borehole core casing and sealed with bentonite. A stable temperature of 1.45 °C was recorded at the base of the borehole in the year following coring (R. Daanen, personal communication). Details of this coring were previously described in brief in ref. 26.

## Lake sediment classification

Cores were capped, sealed and transported to the University of Alaska, Fairbanks (UAF), where they were stored upright at 3 °C. Sediment cores were split in August 2018 and described, photographed and subsampled by a team of researchers. Half of each split core was used for sample collection and half was stored as an archive at UAF. An 18 Ga (1.2 mm) shear drill was used to open each side of the plastic core liners, and cores were divided in half vertically by drawing a piece of fishing line through the cut liner. Exposed core surfaces were gently scraped with a sterilized metal pastry plate to remove the thin layer of water and sediment that may have been pulled down the length of the core during slicing. GSL cores were described with respect to thickness of lake surface sediments and underlying silt and sand/gravel horizons.

As described in ref. 26, macro plant remains were hand-picked across the sediment cores for radiocarbon dating. $^{14}C$ dates were obtained via accelerator mass spectrometry, using the mini carbon dating system at AWI Bremerhaven and results were calibrated using the CALIB 7.1 with the IntCal13 dataset[50,51]. Uncalibrated ages (yr BP) and calibrated ages (cal yr BP, rounded) are reported alongside ±2 s.d. confidence ranges (Table 1).

Shallow (0–5 m), intermediate (6–15 m) and deep (16–20 m) sediment depth classifications were determined based on $^{14}C$ dating and sediment descriptions (Table 1), sediment characteristics (Table 2), and following other studies[1,21,23,31,35,43]. Shallow depths correspond to sediments deposited after inundation and burial of the 1 m depth basal trash layer (the former forest floor[26]), and also include underlying layered silt and organic-rich inclusions down to 5 m depth (inclusive). Recent literature has distinguished shallow sediments as 0–3 m depth[2,44]; we included GSL sediments down to 5 m in our analysis because sediment collected at 5.24–5.39 m probably represented an integrated sample of mineral and organic-rich sediments from overlying horizons. The $^{14}C$ date of the macrofossil in this horizon was the same as the 1 m basal trash layer macrofossil, and in this particular coring section we observed mixing of sediments due to sloughing of material from the inner walls of the casing. We subsequently avoided this source of potential contamination by cleaning the casing in-between deeper drives. The underlying intermediate depths consisted of silt-dominated, late Pleistocene Yedoma sediments, and the deep depths were composed of unconsolidated fluvial sediments that are probably early-to-middle Pleistocene Fox Gravel.

## Lake sediment sampling

Cut-off syringes were used to obtain 5 ml sediment plugs at 150 depths for per cent moisture, bulk density, magnetic susceptibility, macrofossils, total nitrogen ($N_{tot}$), total C ($C_{tot}$), total organic C ($C_{org}$), total inorganic C ($C_{inorg}$), $^{14}C$ dating and $\delta^{13}C$. Sediment plugs were taken every 5–10 cm from the shallow cores, and every 10–20 cm from the deep cores. Bulk density subsamples were stored at 4 °C and remaining subsamples were frozen immediately upon collection. Sample analysis was conducted at the University of Potsdam.

For laboratory incubations, 150–200 g of sediment was taken from 35 selected depths. At each sampling location, sediment was collected in a sterile Whirl-Pak bag between two points that spanned 14–16 cm of vertical core depth. The unsealed Whirl-Pak bag was inserted into a larger aluminium tubular film bag (Schlauchfolie aus Alu-Verbund, Gruber-Folien GmbH & Co. KG). Aluminium bags were sealed using electric, heat-sealing tongs and flushed with $N_2$ gas for 2 min to maintain anoxic sediment environments. All samples were stored and shipped at 4 °C to Lawrence Berkeley National Lab.

After sampling, remaining core material was sealed in oxygen barrier film (Krehalon CB100, PVDC film, Filcon), labelled, wrapped in plastic Saran wrap and stored at 4 °C at UAF. No sediment was collected within 1 cm of the plastic core liner; it was assumed that the core's periphery could have been contaminated by the coring instrument, or that shallower material could have been pulled down along the liner. Visibly oxidized areas along the core liner and within the sediment were avoided during sampling.

## Lake sediment incubations

Parallel aerobic and anaerobic incubations were conducted at Lawrence Berkeley National Lab for 12 of the sample depths collected from the core. The 12 depths provided as much vertical coverage of the sediment as possible (given the quantity of sediment available for processing replicates and treatment conditions), and spanned different palaeoconditions of the core (based on sediment depth classifications and $^{14}C$ sampling sites; Table 1). Aerobic serum bottles were incubated under C-free air, and anaerobic bottles under $N_2$ gas. Three temperature treatments selected for incubations (4 °C, 10 °C, 20 °C) bracketed possible future temperature changes across the sediment column[52], and

were consistent with GSL lake sediment temperatures[32] and previous permafrost incubation studies[31,43,53,54]. All 12 depths were incubated at 4 °C, and 5 of the 12 depths were also incubated at 10 °C and 20 °C. Each set of headspace and temperature treatments was incubated in triplicate (132 total incubation bottles).

For 24 h prior to sediment separation, 120 ml serum bottles (borosilicate glass, Wheaton) were degassed in an $N_2$ hood (97% $N_2$ + 3% $H_2$). Aluminium bags containing sediment were opened in the $N_2$ hood and subsampled for gravimetric moisture content analysis—samples were later weighed, oven-dried at 105 °C for 48 h and reweighed. A quantity of 10 g sediment was inserted into each bottle from 10 of the 12 depths; 5 g sediment was used from depths 0.31–0.47 m and 5.24–5.39 m, where less sediment was available. To disturb the sediment as little as possible and maintain intact soil aggregates, sediments were neither sieved nor homogenized as sediment slurries. Instead, sediment was subsampled randomly across the available material to capture the heterogeneity of the 14–16 cm of core depth in each sample bag, and to minimize differences in substrate characteristics across the replicates.

Bottles were capped with butyl rubber stoppers (20 mm, Geo-Microbial Technologies, Inc.), sealed with aluminium crimp tops (20 mm, Thermo Scientific) and weighed. Serum bottles were pre-incubated at their respective temperatures for 5 days to equilibrate after the disturbance of the sampling process. Aerobic bottles were then flushed with C-free air (ProSpec Ultra Zero Air, Praxair) and anaerobic bottles were flushed with $N_2$ gas (Praxair) for 3 min at 1 L $min^{-1}$ prior taking initial headspace gas samples to begin the incubations. Incubations were run for 365 days.

At each sampling time point, 7 ml of gas was collected from the headspace of every bottle using a syringe and was inserted into pre-evacuated 5 ml headspace vials (MicroSolv). Vial evacuations were performed with a vacuum manifold coupled with an SH 071 turbomolecular pumping station. A quantity of 3 ml gas from vials was analysed for GHG concentrations via manual injection gas chromatography on a Shimadzu GC 2014 (Shimadzu Corporation). The gas volume pulled from each incubation bottle was replaced by an equal volume of C-free air or $N_2$ to maintain appropriate oxic/anoxic conditions for microbial communities and to keep serum bottle pressure at equilibrium. Bottles were sampled twice per week for the first month to capture the initial respiration responses; sampling was then gradually scaled down to once per month for the final 5 months as production rates stabilized.

Aerobic bottles were flushed once when $CO_2$ concentrations approached 20,000 ppm, approximately halfway through the incubations. Incubation bottles were periodically weighed to check for sediment moisture loss and to compare to pre- and post-incubation gravimetric water content. After the 365-day incubations, sediment was destructively harvested, weighed, oven-dried (55 °C for 48 h, 105 °C for 48 h), reweighed, ground and homogenized (roller mill and SPEX Certiprep 8000 M Mixer Mill) for solid phase analysis.

## Data analysis

Raw $CO_2$ and $CH_4$ concentrations at each sampling time point were determined by gas chromatography analysis throughout the incubations. Every gas sample taken from a bottle represented the accumulated amount of $CO_2$ and $CH_4$ respired up until that day, diluted by 7 ml per time point since the beginning of the incubations. To calculate a running total amount of $CO_2$ and $CH_4$ respired by each jar over the course of the incubations, we converted raw GHG concentrations in each bottle from parts per million to micrograms using the ideal gas law, and corrected for the 7 ml headspace dilution per time point.

Here we report carbon respiration in four ways. (1) Cumulative carbon respired by type of gas. This was calculated as the average production of the analytical replicates within each temperature treatment for the final three incubation time points ($n$ = 9), normalized by initial quantity of SOC (for example, mg C-$CO_2$ $gC^{-1}$) and by dry weight (for example, ug C-$CO_2$ $gdw^{-1}$). (2) Total carbon respired. C-$CO_2$ and C-$CH_4$ respiration were summed for each incubation jar per time point (for example, mg C-$CO_2$ $gC^{-1}$ + mg C-$CH_4$ $gC^{-1}$). Averages were then taken for analytical replicates within each temperature treatment for the final three incubation time points ($n$ = 18). (3) Total C-$CO_2$e respired. C-$CH_4$ respiration per time point was converted to carbon equivalents (C-$CO_2$e) using a $GWP_{100}$ of 28. We used this $GWP_{100}$ due to uncertainties related to including climate–carbon feedbacks in estimates, and acknowledge that this may provide a low estimate of the full effects of $CH_4$ on $CO_2$e at each depth[55]. C-$CO_2$ and C-$CH_4$ as C-$CO_2$e respiration was then summed for each incubation jar by time point (for example, mg C-$CO_2$ $gC^{-1}$ + mg C-$CO_2$e $gC^{-1}$). Averages were taken for analytical replicates within each temperature treatment for the final three incubation time points ($n$ = 18). (4) Sediment column production potentials. Using sediment bulk density, the cumulative carbon respired by type of gas and normalized per gram dry weight (1), and the vertical distance of each depth increment (shallow: 0–5.99 m; intermediate: 5.99–15.99 m; deep: 15.99–19.99 m), production potentials were calculated for all analytical replicates within each depth increment, temperature treatment, and headspace treatment on a daily and annual basis (for example, g C-$CO_2$ $m^2$ $d^{-1}$, g C-$CO_2$ $m^2$ $y^{-1}$; $n$ = variable by depth–temperature combination; see Table 2).

To determine the temperature sensitivity of C-$CO_2$, C-$CH_4$ and C-$CO_2$e respiration, $Q_{10}$ coefficients were calculated for the five sediment depths exposed to all three incubation temperatures. This was done for early, middle and end periods of the incubations (days 30, 150 and 365, respectively) using data from three time points that bracketed each period (for example, anaerobic $Q_{10}$ coefficients were calculated for day 30 using data from days 26, 28 and 33). We report $Q_{10}$ coefficients in terms of cumulative respiration, rather than respiration rates, to account for lag times associated with $CH_4$ production[37,38]. These values thus represent the factor by which the amount of gas produced changed, given a 10 °C increase in temperature. Some early cumulative C-$CH_4$ data points were dropped from the calculations because the log-transformed regression analyses could not account for zero values ($Q_{10}$ value significance is noted in Fig. 2). Cumulative respiration was not averaged across or within replicates to find $Q_{10}$ values; all replicate data were included for each time point.

The following equations were used to calculate $Q_{10}$ coefficients[56]:

An exponential equation describes the relationship between soil respiration and temperature, where $R_T$ is the soil respiration rate at a given temperature $T$ (°C), $R_0$ is a reference respiration rate where $T$ = 0 °C, $e$ is the exponential constant and $\beta$ is the temperature coefficient of the reaction:

$$R_T = R_0 \times e^{\beta T} \quad (1)$$

The $Q_{10}$ coefficient of soil respiration describes the change in respiration rate under an increase of $T$ = 10 °C, where $R_T$ and $R_{T+10}$ are the rates of respiration under temperatures $T$ and $T$ + 10:

$$Q_{10} = R_{T+10}/R_T \quad (2)$$

The $Q_{10}$ value can be calculated as the slope of the relationship between soil respiration and temperature:

$$\text{slope} = Q_{10} = [R_0 \times e^{\beta(T+10)}]/[R_0 \times e^{\beta T}] = e^{10\beta} \quad (3)$$

To account for the exponential fit of our data, we took the slope of a linear regression between the log-transformed cumulative respiration and temperature (equation (4)) and used this to calculate the $Q_{10}$ coefficients (equation (5)):

$$\text{Slope} = \ln R_{T+10} - \ln R_T \quad (4)$$

$$Q_{10} = e^{\ln(\text{slope})\times 10} \quad (5)$$

Four time points were dropped from aerobic and anaerobic $CO_2$ data (days 99–117 and days 167–223, respectively), as they were deemed implausible due to negative fluxes. We did not use these data and assumed zero respiration at those time points. $CH_4$ data were kept in the original data set because (1) most jars had no change in headspace concentration over this time (effectively zero flux); and (2) jars that did have $CH_4$ production did not show depreciable headspace concentrations. Additional details can be found within our raw data and code[57].

To determine the potential productivity of expanding Yedoma-type lakes across the Arctic, we extrapolated annual GSL whole sediment column production to the broader Arctic region. The following calculations were used:

Annual sediment column production was calculated as a combined (one-third) aerobic potential production plus (two-thirds) anaerobic production at 4 °C (g C $m^{-2}$ $y^{-1}$). We assumed anaerobic conditions would prevail over aerobic, which is typical of talik below thermokarst lakes. Although shallow sediments are already experiencing markedly warmer seasonal temperature fluctuations than the 4 °C values used here[31], temperatures below 3 m depth remain close to freezing and represent a larger portion of the full sediment column:

$$\text{Annual sediment column production} = \left[1/3 \times \sum \text{aer. sed. col. prod.}_{4\,^{\circ}\text{C}}\right] + \left[2/3 \times \sum \text{ana. sed. col.prod.}_{4\,^{\circ}\text{C}}\right] \quad (6)$$

Following previous studies[1,13], we calculated that 5–15% of potential sediment production was emitted to the atmosphere:

$$\text{Annual sediment column production}_{5-15\%} = \text{equation}(6) \times (0.05 \text{ or } 0.15) \quad (7)$$

We used a value of 150,000 $km^2$ to represent the area of the disturbed Yedoma domain currently covered by lakes and rivers and underlain by unfrozen deposits[58]. The annual productivity (Pg C $yr^{-1}$) of expanding Yedoma-type lakes in the Arctic would therefore be:

$$\text{Annual productivity of expanding lakes} = \text{equation}\,(7) \times (1.5 \times 10^{11})\text{m}^2 \times (1.0 \times 10^{-15})\text{Pg C} \quad (8)$$

Additionally, time series flux data over the length of the incubations and temperature sensitivity ratios are available in the raw data and code[57].

### Statistics

For reported average carbon respiration values, standard errors are included for analytical replicates per sample depth, headspace treatment and temperature treatment.

For $Q_{10}$ coefficients, we used linear models to determine the slope of log-transformed cumulative respiration versus temperature for C-$CO_2$, C-$CH_4$ and C-$CO_2$e, extracted summary statistics for each model, and calculated $Q_{10}$ values. The fit of the linear models was evaluated using residual versus fitted plots, $Q$–$Q$ plots and density plots. Significant ($P < 0.05$) $Q_{10}$ values are displayed as solid points (Fig. 2a,b), while insignificant values are displayed as open points (insignificance was largely driven by negligible or variable C-$CH_4$ contributions). A multivariate linear regression was also used to analyse the effects of incubation time period and sediment depth on $Q_{10}$ temperature sensitivities.

All data processing and statistics were done in R (version 4.1.0).

### Reporting summary

Further information on research design is available in the Nature Portfolio Reporting Summary linked to this article.

## Data availability

The data that support the findings of this study are archived and freely available through the ESS-DIVE repository at https://doi.org/10.15485/2336866.

## Code availability

The R code used to generate the results of this study is archived and freely available through the ESS-DIVE repository at https://doi.org/10.15485/2336866.

## References


45. Lindgren, P. R., Grosse, G., Walter Anthony, K. M. & Meyer, F. J. Detection and spatiotemporal analysis of methane ebullition on thermokarst lake ice using high-resolution optical aerial imagery. *Biogeosciences* **13**, 27–44 (2016).
46. Brosius, L. S. et al. Using the deuterium isotope composition of permafrost meltwater to constrain thermokarst lake contributions to atmospheric $CH_4$ during the last deglaciation. *J. Geophys. Res. Biogeosci.* https://doi.org/10.1029/2011JG001810 (2012).
47. Pastick, N. J. et al. Distribution of near-surface permafrost in Alaska: estimates of present and future conditions. *Remote Sens. Environ.* **168**, 301–315 (2015).
48. Jorgenson, T. et al. Permafrost characteristics of Alaska. In *Proc. 9th International Conference on Permafrost* (Institute of Northern Engineering, University of Alaska Fairbanks, 2008).
49. Gagné, K. R. et al. Composition and photo-reactivity of organic matter from permafrost soils and surface waters in interior Alaska. *Environ. Sci. Process. Impacts* **22**, 1525–1539 (2020).
50. Stuiver, M. & Reimer, P. J. Extended $^{14}C$ Data base and revised CALIB 3.0 $^{14}C$ age calibration program. *Radiocarbon* **35**, 215–230 (1993).
51. Synal, H. A., Stocker, M. & Suter, M. MICADAS: a new compact radiocarbon AMS system. *Nucl. Instrum. Methods Phys. Res. B* **259**, 7–13 (2007).
52. Heslop, J. K. et al. A synthesis of methane dynamics in thermokarst lake environments. *Earth-Sci. Rev.* **210**, 103365 (2020).
53. Treat, C. C. et al. A pan-Arctic synthesis of $CH_4$ and $CO_2$ production from anoxic soil incubations. *Glob. Change Biol.* **21**, 2787–2803 (2015).
54. Treat, C. C. et al. Temperature and peat type control $CO_2$ and $CH_4$ production in Alaskan permafrost peats. *Glob. Change Biol.* **20**, 2674–2686 (2014).
55. Myhre, G. et al. in *Climate Change 2013: The Physical Science Basis* (eds Stocker, T. F. et al.) 659–740 (IPCC, Cambridge Univ. Press, 2013).
56. Tang, J., Cheng, H. & Fang, C. The temperature sensitivity of soil organic carbon decomposition is not related to labile and recalcitrant carbon. *PLoS ONE* **12**, e0186675 (2017).
57. Freitas, N. L., Walter Anthony, K. M., Lenz, J., Porras, R. C. & Torn, M. S. Substantial and overlooked greenhouse gas emissions from deep Arctic lake sediment - supporting data and code. *ESS-DIVE* https://data.ess-dive.lbl.gov/datasets/doi:10.15485/2336866 (2024).
58. Strauss, J. et al. The deep permafrost carbon pool of the Yedoma region in Siberia and Alaska. *Geophys. Res. Lett.* **40**, 6165–6170 (2013).


## Acknowledgements

This material is based upon work supported by the National Science Foundation Graduate Research Fellowship Program under grant no. DGE 1752814 (N.L.F.); by NSF P2C2 1903735 (K.W.A.); and by the Next-Generation Ecosystem Experiments (NGEE Arctic) project, which is supported by the Office of Biological and Environmental Research in the DOE Office of Science, and other Office of Science support to Lawrence Berkeley National Lab under contract no. DE-AC02-

05CH11231 (M.S.T., N.L.F.). C. Mayo assisted with field work, and C. Mayo and J. Guerard provided lab space at UAF. G. Grosse and S. Liebner assisted with data interpretation. The late R. Daanen and the late D. Brotherton also assisted with field work, and we additionally recognize them here for their lasting contributions to Arctic research.

## Author contributions

K.W.A. and J.L. initiated the project, designed the sampling campaign and carried out the sediment coring. N.L.F. and J.L. subsampled the sediment. J.L. conducted sediment classification, geochemical analyses and prepared samples for $^{14}C$ dating. N.L.F. conducted the year-long incubation study with assistance from R.C.P., and analysed and interpreted the data with assistance from M.S.T. and K.W.A. N.L.F. wrote the manuscript, and M.S.T., K.W.A., J.L. and R.C.P. commented on and contributed to manuscript revisions.

## Competing interests

The authors declare no competing interests.

## Additional information

**Extended data** is available for this paper at https://doi.org/10.1038/s41561-024-01614-y.

**Supplementary information** The online version contains supplementary material available at https://doi.org/10.1038/s41561-024-01614-y.

**Correspondence and requests for materials** should be addressed to Nancy L. Freitas or Margaret S. Torn.

**Peer review information** *Nature Geoscience* thanks Christina Biasi and the other, anonymous, reviewer(s) for their contribution to the peer review of this work. Primary Handling Editor: Xujia Jiang, in collaboration with the *Nature Geoscience* team.

https://doi.org/10.1038/s41561-024-01614-y

## Extended Data Table 1 | C-$CO_2$, C-$CH_4$, total carbon, and C-$CO_2$e production normalized by dry weight of sediment, by day ~365 of the incubations

| | | Cumulative respiration * (ug C-$CO_2$ $gdw^{-1}$) | | Cumulative respiration * (ug C-$CH_4$ $gdw^{-1}$) | | Total C respired ** (ug C $gdw^{-1}$) | | Total C-$CO_2$e respired *** (ug C-$CO_2$e $gdw^{-1}$) | |
|---|---|---|---|---|---|---|---|---|---|
| Sample depth range (m) | Temperature treatment (°C) | Aerobic | Anaerobic | Aerobic | Anaerobic | Aerobic | Anaerobic | Aerobic | Anaerobic |
| 0.31 - 0.47 | 4 | 63.32 (1.26) | 42.74 (1.19) | 7.93E-2 (4.94E-3) | 1.89E-1 (6.74E-3) | 63.40 (1.26) | 42.93 (1.19) | 64.13 (1.29) | 44.68 (1.22) |
| 0.31 - 0.47 | 10 | 97.23 (2.16) | 65.54 (1.78) | 2.59E-1 (9.77E-3) | 2.48E-1 (9.56E-3) | 97.49 (2.16) | 65.79 (1.78) | 99.88 (2.21) | 68.08 (1.80) |
| 0.31 - 0.47 | 20 | 168.29 (2.74) | 112.31 (2.86) | 1.96E-1 (7.04E-3) | 3.94E-1 (9.47E-3) | 168.48 (2.74) | 112.70 (2.86) | 170.29 (2.73) | 116.33 (2.84) |
| 0.60 - 0.76 | 4 | 1920.63 (60.21) | 581.13 (15.65) | 7.61E-1 (2.69E-2) | 93.28 (5.04) | 1921.39 (60.22) | 674.42 (16.10) | 1928.40 (60.36) | 1533.09 (52.66) |
| 1.10 - 1.17 | 4 | 384.23 (7.82) | 177.84 (4.04) | 8.39E-2 (5.94E-3) | 2.21E-1 (1.49E-2) | 384.31 (7.82) | 178.06 (4.03) | 385.09 (7.85) | 180.09 (4.01) |
| 3.05 - 3.21 | 4 | 482.88 (6.51) | 218.01 (4.25) | 1.82E-1 (1.04E-3) | 5.26E-1 (4.62E-3) | 483.06 (6.51) | 218.54 (4.25) | 484.74 (6.51) | 223.38 (4.26) |
| 5.24 - 5.39 | 4 | 139.91 (2.56) | 89.51 (2.82) | 6.28E-2 (5.11E-3) | 2.72E-1 (1.83E-3) | 139.97 (2.56) | 89.78 (2.82) | 140.55 (2.59) | 92.29 (2.83) |
| 5.24 - 5.39 | 10 | 137.21 (2.29) | 96.05 (2.54) | 2.26E-1 (1.03E-2) | 2.74E-1 (2.89E-3) | 137.44 (2.30) | 96.33 (2.54) | 139.52 (2.33) | 98.85 (2.55) |
| 5.24 - 5.39 | 20 | 294.09 (8.39) | 135.54 (3.50) | 1.85E-1 (6.61E-3) | 2.32E-1 (1.11E-2) | 294.28 (8.39) | 135.77 (3.50) | 295.98 (8.43) | 137.91 (3.48) |
| 7.21 - 7.35 | 4 | 136.43 (1.49) | 109.57 (1.89) | 1.32E-1 (1.61E-3) | 1.60E-1 (1.01E-3) | 136.56 (1.49) | 109.73 (1.89) | 137.77 (1.50) | 111.20 (1.90) |
| 10.05 - 10.20 | 4 | 236.31 (7.37) | 133.76 (3.03) | 8.24E-2 (2.75E-3) | 3.73E-1 (3.19E-2) | 236.40 (7.37) | 134.13 (3.02) | 237.16 (7.36) | 137.57 (2.96) |
| 10.05 - 10.20 | 10 | 238.73 (3.25) | 145.22 (2.99) | 1.46E-1 (1.05E-3) | 9.05E-1 (5.22E-2) | 238.88 (3.25) | 146.12 (3.00) | 240.23 (3.26) | 154.45 (3.18) |
| 10.05 - 10.20 | 20 | 267.42 (2.95) | 166.28 (3.78) | 1.68E-1 (2.13E-3) | 11.67 (7.15E-1) | 267.58 (2.94) | 177.95 (4.04) | 269.13 (2.94) | 285.33 (9.13) |
| 12.62 - 12.77 | 4 | 202.14 (9.19) | 120.63 (2.92) | 1.27E-1 (1.01E-3) | 2.77E-1 (2.06E-3) | 202.26 (9.19) | 120.91 (2.92) | 203.43 (9.19) | 123.46 (2.92) |
| 13.65 - 13.80 | 4 | 271.45 (4.94) | 174.34 (5.31) | 1.51E-1 (1.91E-3) | 8.48 (1.23) | 271.60 (4.94) | 182.82 (4.64) | 272.99 (4.95) | 260.91 (10.15) |
| 16.63 - 16.78 | 4 | 314.20 (5.15) | 267.30 (11.91) | 1.61E-1 (9.53E-4) | 4.03 (3.45E-1) | 314.37 (5.15) | 271.33 (11.66) | 315.85 (5.15) | 308.47 (9.57) |
| 18.52 - 18.67 | 4 | 95.65 (3.36) | 99.00 (2.32) | 5.27E-2 (3.32E-3) | 1.02E-1 (2.87E-3) | 95.70 (3.35) | 99.10 (2.32) | 96.19 (3.34) | 100.04 (2.31) |
| 18.52 - 18.67 | 10 | 54.76 (1.54) | 123.68 (2.50) | 5.90E-2 (3.15E-3) | 8.67E-2 (4.93E-3) | 54.82 (1.54) | 123.76 (2.50) | 55.36 (1.54) | 124.56 (2.49) |
| 18.52 - 18.67 | 20 | 100.67 (1.24) | 129.06 (2.38) | 9.74E-2 (1.62E-3) | 10.46 (1.53) | 100.77 (1.24) | 139.52 (2.55) | 101.67 (1.25) | 235.78 (15.33) |
| 19.83 - 19.98 | 4 | 267.04 (9.22) | 158.95 (5.29) | 1.61E-1 (3.64E-3) | 24.95 (8.57E-1) | 267.20 (9.22) | 183.91 (5.45) | 268.69 (9.24) | 413.60 (10.70) |
| 19.83 - 19.98 | 10 | 290.26 (9.72) | 178.05 (5.60) | 1.86E-1 (1.06E-3) | 141.02 (6.46) | 290.45 (9.72) | 319.07 (10.36) | 292.16 (9.71) | 1617.16 (68.78) |
| 19.83 - 19.98 | 20 | 467.24 (12.90) | 262.08 (6.59) | 1.89E-1 (1.01E-3) | 103.06 (8.14E-1) | 467.42 (12.90) | 365.14 (7.17) | 469.17 (12.91) | 1313.82 (13.69) |

Standard error reported in parentheses. * Cumulative respiration columns calculate average production of the analytical replicates within each temperature treatment for the final three incubation time points ($n = 9$), normalized by dry weight of sediment. ** Total C respired was calculated as the sum of cumulative C-$CO_2$ and C-$CH_4$ respiration ($n = 18$) across the final three time points. *** Total C-$CO_2$e respired was calculated as the sum of cumulative C-$CO_2$ and C-$CH_4$ [as C-$CO_2$e, using a $GWP_{100}$ of 28] respiration ($n = 18$) across the final three time points.

https://doi.org/10.1038/s41561-024-01614-y

## Extended Data Table 2 | C-$CO_2$, C-$CH_4$, total carbon, and C-$CO_2$e production normalized by initial quantity SOC, by day ~365 of the incubations

| | | Cumulative respiration * (mg C-$CO_2$ $gC^{-1}$) | | Cumulative respiration * (mg C-$CH_4$ $gC^{-1}$) | | Total C respired ** (mg C $gC^{-1}$) | | | Total C-$CO_2$e respired *** (mg C-$CO_2$e $gC^{-1}$) | | |
|---|---|---|---|---|---|---|---|---|---|---|---|
| Sample depth range (m) | Temperature treatment (°C) | Aerobic | Anaerobic | Aerobic | Anaerobic | Aerobic | Anaerobic | Aerobic : Anaerobic | Aerobic | Anaerobic | Aerobic : Anaerobic |
| 0.31 - 0.47 | 4 | 6.06 (0.12) | 4.09 (0.11) | 7.59E-3 (4.73E-4) | 1.81E-2 (6.45E-4) | 6.07 (0.12) | 4.11 (0.11) | 1.48 | 6.14 (0.12) | 4.28 (0.12) | 1.43 |
| 0.31 - 0.47 | 10 | 9.31 (0.21) | 6.27 (0.17) | 2.48E-2 (9.35E-4) | 2.38E-2 (9.15E-4) | 9.33 (0.21) | 6.29 (0.17) | 1.48 | 9.56 (0.22) | 6.51 (0.18) | 1.47 |
| 0.31 - 0.47 | 20 | 16.11 (0.26) | 10.75 (0.27) | 1.88E-2 (6.74E-4) | 3.77E-2 (9.06E-4) | 16.13 (0.26) | 10.79 (0.27) | 1.49 | 16.30 (0.27) | 11.13 (0.28) | 1.46 |
| 0.60 - 0.76 | 4 | 4.85 (0.15) | 1.47 (0.04) | 1.92E-3 (6.81E-5) | 2.36E-1 (1.27E-2) | 4.85 (0.15) | 1.71 (0.05) | 2.84 | 4.87 (0.15) | 3.88 (0.17) | 1.26 |
| 1.10 - 1.17 | 4 | 1.25 (0.03) | 0.58 (0.01) | 2.73E-4 (1.93E-5) | 7.19E-4 (4.85E-5) | 1.25 (0.03) | 0.58 (0.01) | 2.16 | 1.25 (0.03) | 0.59 (0.01) | 2.12 |
| 3.05 - 3.21 | 4 | 26.35 (0.36) | 11.90 (0.23) | 9.93E-3 (5.69E-5) | 2.87E-2 (2.52E-4) | 26.36 (0.36) | 11.93 (0.23) | 2.21 | 26.45 (0.36) | 12.19 (0.23) | 2.17 |
| 5.24 - 5.39 | 4 | 3.63 (0.07) | 2.32 (0.07) | 1.63E-3 (1.33E-4) | 7.05E-3 (4.76E-5) | 3.63 (0.07) | 2.33 (0.07) | 1.56 | 3.65 (0.07) | 2.39 (0.07) | 1.53 |
| 5.24 - 5.39 | 10 | 3.56 (0.06) | 2.49 (0.07) | 5.87E-3 (2.68E-4) | 7.10E-3 (7.48E-5) | 3.57 (0.06) | 2.50 (0.07) | 1.43 | 3.62 (0.06) | 2.56 (0.07) | 1.41 |
| 5.24 - 5.39 | 20 | 7.63 (0.22) | 3.52 (0.09) | 4.80E-3 (1.71E-4) | 6.02E-3 (2.89E-4) | 7.63 (0.22) | 3.53 (0.09) | 2.16 | 7.68 (0.22) | 3.58 (0.09) | 2.15 |
| 7.21 - 7.35 | 4 | 136.43 (1.49) | 109.57 (1.89) | 1.32E-1 (1.61E-3) | 1.60E-1 (1.01E-3) | 136.56 (1.49) | 109.73 (1.89) | 1.24 | 137.78 (1.51) | 111.20 (1.90) | 1.24 |
| 10.05 - 10.20 | 4 | 26.58 (0.83) | 15.05 (0.34) | 9.27E-3 (3.10E-4) | 4.20E-2 (3.59E-3) | 26.59 (0.83) | 15.09 (0.34) | 1.76 | 26.67 (0.83) | 15.48 (0.38) | 1.72 |
| 10.05 - 10.20 | 10 | 26.85 (0.37) | 16.33 (0.34) | 1.65E-2 (1.18E-4) | 1.02E-1 (5.87E-3) | 26.87 (0.37) | 16.43 (0.35) | 1.64 | 27.02 (0.37) | 17.37 (0.40) | 1.56 |
| 10.05 - 10.20 | 20 | 30.08 (0.33) | 18.70 (0.42) | 1.89E-2 (2.40E-4) | 1.31 (8.04E-2) | 30.10 (0.33) | 20.01 (0.50) | 1.50 | 30.27 (0.33) | 32.10 (1.24) | 0.94 |
| 12.62 - 12.77 | 4 | 24.95 (1.13) | 14.89 (0.36) | 1.57E-2 (1.25E-4) | 3.42E-2 (2.55E-4) | 24.97 (1.13) | 14.92 (0.36) | 1.67 | 25.11 (1.13) | 15.24 (0.36) | 1.65 |
| 13.65 - 13.80 | 4 | 13.97 (0.25) | 8.97 (0.27) | 7.75E-3 (9.81E-5) | 4.36E-1 (6.34E-2) | 13.98 (0.25) | 9.41 (0.33) | 1.49 | 14.05 (0.25) | 13.42 (0.92) | 1.05 |
| 16.63 - 16.78 | 4 | 10.24 (0.17) | 8.71 (0.39) | 5.25E-3 (3.11E-5) | 1.32E-1 (1.12E-2) | 10.25 (0.17) | 8.84 (0.40) | 1.16 | 10.29 (0.17) | 10.05 (0.51) | 1.02 |
| 18.52 - 18.67 | 4 | 95.65 (3.36) | 99.00 (2.32) | 5.27E-2 (3.32E-3) | 1.02E-1 (2.87E-3) | 95.70 (3.36) | 99.10 (2.32) | 0.97 | 96.19 (3.39) | 100.04 (2.35) | 0.96 |
| 18.52 - 18.67 | 10 | 54.76 (1.54) | 123.68 (2.50) | 5.90E-2 (3.15E-3) | 8.67E-2 (4.93E-3) | 54.82 (1.54) | 123.77 (2.50) | 0.44 | 55.36 (1.57) | 124.57 (2.55) | 0.44 |
| 18.52 - 18.67 | 20 | 100.67 (1.24) | 129.06 (2.38) | 9.74E-2 (1.62E-3) | 10.46 (1.53) | 100.77 (1.24) | 139.56 (3.91) | 0.72 | 101.66 (1.26) | 236.06 (17.98) | 0.43 |
| 19.83 - 19.98 | 4 | 10.33 (0.36) | 6.15 (0.20) | 6.24E-3 (1.41E-4) | 9.65E-1 (3.31E-2) | 10.34 (0.36) | 7.12 (0.23) | 1.45 | 10.39 (0.36) | 16.00 (0.54) | 0.65 |
| 19.83 - 19.98 | 10 | 11.22 (0.38) | 6.88 (0.22) | 7.20E-3 (4.11E-5) | 5.45 (2.50E-1) | 11.23 (0.38) | 12.33 (0.47) | 0.91 | 11.29 (0.38) | 62.48 (2.77) | 0.18 |
| 19.83 - 19.98 | 20 | 18.07 (0.50) | 10.13 (0.25) | 7.33E-3 (3.92E-5) | 3.98 (3.15E-2) | 18.08 (0.50) | 14.11 (0.28) | 1.28 | 18.14 (0.50) | 50.83 (0.57) | 0.36 |

Standard error reported in parentheses. * Cumulative respiration columns calculate average production of the analytical replicates within each temperature treatment for the final three incubation time points ($n = 9$), normalized by initial quantity of SOC. ** Total C respired was calculated as the sum of cumulative C-$CO_2$ and C-$CH_4$ respiration ($n = 18$), and includes the ratio between average aerobic and anaerobic production across the final three time points. *** Total C-$CO_2$e respired was calculated as the sum of cumulative C-$CO_2$ and C-$CH_4$ [as C-$CO_2$e, using a $GWP_{100}$ of 28] respiration ($n = 18$), and includes the ratio between average aerobic and anaerobic production across the final three time points.

https://doi.org/10.1038/s41561-024-01614-y

## Extended Data Table 3 | Summary statistics for C-$CO_2$, C-$CH_4$, and C-$CO_2$e production, by day ~365 of the incubations

| | | $C\text{-}CO_2$ : $C\text{-}CH_4$ | | $C\text{-}CO_2$ : $C\text{-}CH_4$ [as $C\text{-}CO_2e$] | | Percent $C\text{-}CO_2$ of $C\text{-}CO_2e$ (%) | | Percent $C\text{-}CH_4$ [as $C\text{-}CO_2e$] of $C\text{-}CO_2e$ (%) | | Percent of initial SOC mineralized (%) | |
|---|---|---|---|---|---|---|---|---|---|---|---|
| Sample depth range (m) | Temperature treatment (°C) | Aerobic | Anaerobic | Aerobic | Anaerobic | Aerobic | Anaerobic | Aerobic | Anaerobic | Aerobic | Anaerobic |
| 0.31 - 0.47 | 4 | 798.42 | 225.97 | 78.19 | 22.11 | 98.70 | 95.56 | 1.26 | 4.32 | 0.61 | 0.41 |
| 0.31 - 0.47 | 10 | 375.40 | 263.45 | 36.80 | 25.91 | 97.38 | 96.31 | 2.65 | 3.72 | 0.93 | 0.63 |
| 0.31 - 0.47 | 20 | 856.91 | 285.15 | 83.91 | 27.99 | 98.83 | 96.59 | 1.18 | 3.45 | 1.61 | 1.08 |
| 0.60 - 0.76 | 4 | 2526.04 | 6.23 | 247.45 | 0.61 | 99.59 | 37.89 | 0.40 | 62.11 | 0.49 | 0.17 |
| 1.10 - 1.17 | 4 | 4578.75 | 806.68 | 448.03 | 79.02 | 100.00 | 98.31 | 0.22 | 1.24 | 0.13 | 0.06 |
| 3.05 - 3.21 | 4 | 2653.58 | 414.63 | 260.89 | 40.61 | 99.62 | 97.62 | 0.38 | 2.40 | 2.64 | 1.19 |
| 5.24 - 5.39 | 4 | 2226.99 | 329.08 | 218.67 | 32.22 | 99.45 | 97.07 | 0.45 | 3.01 | 0.36 | 0.23 |
| 5.24 - 5.39 | 10 | 606.47 | 350.70 | 59.43 | 34.34 | 98.34 | 97.27 | 1.65 | 2.83 | 0.36 | 0.25 |
| 5.24 - 5.39 | 20 | 1589.58 | 584.72 | 155.71 | 57.24 | 99.35 | 98.32 | 0.64 | 1.72 | 0.76 | 0.35 |
| 7.21 - 7.35 | 4 | 1033.56 | 684.81 | 101.06 | 67.22 | 99.02 | 98.53 | 0.98 | 1.47 | 13.66 | 10.97 |
| 10.05 - 10.20 | 4 | 2867.31 | 358.33 | 280.97 | 35.16 | 99.66 | 97.22 | 0.35 | 2.76 | 2.66 | 1.51 |
| 10.05 - 10.20 | 10 | 1627.27 | 160.10 | 159.82 | 15.70 | 99.37 | 94.01 | 0.62 | 5.99 | 2.69 | 1.64 |
| 10.05 - 10.20 | 20 | 1591.53 | 14.27 | 155.85 | 1.40 | 99.37 | 58.26 | 0.64 | 41.74 | 3.01 | 2.00 |
| 12.62 - 12.77 | 4 | 1589.17 | 435.38 | 155.94 | 42.66 | 99.36 | 97.70 | 0.64 | 2.29 | 2.50 | 1.49 |
| 13.65 - 13.80 | 4 | 1802.58 | 20.57 | 176.61 | 2.02 | 99.43 | 66.84 | 0.56 | 33.16 | 1.40 | 0.94 |
| 16.63 - 16.78 | 4 | 1950.48 | 65.98 | 191.40 | 6.50 | 99.51 | 86.67 | 0.52 | 13.33 | 1.02 | 0.88 |
| 18.52 - 18.67 | 4 | 1814.99 | 970.59 | 177.79 | 95.19 | 99.44 | 98.96 | 0.56 | 1.04 | 9.57 | 9.91 |
| 18.52 - 18.67 | 10 | 928.14 | 1426.53 | 90.96 | 139.75 | 98.92 | 99.29 | 1.09 | 0.71 | 5.48 | 12.38 |
| 18.52 - 18.67 | 20 | 1033.57 | 12.29 | 101.28 | 1.21 | 99.03 | 54.67 | 0.98 | 45.33 | 10.08 | 13.95 |
| 19.83 - 19.98 | 4 | 1655.45 | 6.37 | 162.17 | 0.62 | 99.42 | 38.44 | 0.61 | 61.56 | 1.03 | 0.71 |
| 19.83 - 19.98 | 10 | 1558.33 | 1.26 | 152.65 | 0.12 | 99.38 | 11.01 | 0.65 | 88.99 | 1.12 | 1.23 |
| 19.83 - 19.98 | 20 | 2465.21 | 2.55 | 241.58 | 0.25 | 99.61 | 19.93 | 0.41 | 80.07 | 1.81 | 1.41 |

Ratios and percentages of average production between various gasses. Average production values were calculated for analytical replicates within each temperature treatment across the final three incubation time points ($n = 9$). Note that rounding differences account for the fact that a few $C\text{-}CO_2$ and $C\text{-}CH_4$ percentages do not sum exactly to 100%.

https://doi.org/10.1038/s41561-024-01614-y

## Extended Data Table 4 | Daily and annual sediment column production potentials for cumulative C-$CO_2$, C-$CH_4$, and total carbon

| | | $CO_2$ production (g C-$CO_2$ $m^{-2}$ $d^{-1}$) | | $CH_4$ production (g C-$CH_4$ $m^{-2}$ $d^{-1}$) | | Total C production (g C $m^{-2}$ $d^{-1}$) | | $CO_2$ production (g C-$CO_2$ $m^{-2}$ $y^{-1}$) | | $CH_4$ production (g C-$CH_4$ $m^{-2}$ $y^{-1}$) | | Total C production (g C $m^{-2}$ $y^{-1}$) | |
|---|---|---|---|---|---|---|---|---|---|---|---|---|---|
| Sediment depth range (m) | Temperature treatment (°C) | Aerobic | Anaerobic | Aerobic | Anaerobic | Aerobic | Anaerobic | Aerobic | Anaerobic | Aerobic | Anaerobic | Aerobic | Anaerobic |
| 0.00 - 5.99 | 4 | 3.71 | 1.76 | 1.61E-03 | 2.83E-02 | 3.71 | 1.79 | 1353.54 | 642.25 | 0.59 | 10.31 | 1354.12 | 652.56 |
| 5.99 - 15.99 | 4 | 8.41 | 5.37 | 4.94E-03 | 8.54E-02 | 8.42 | 5.45 | 3070.97 | 1959.37 | 1.80 | 31.15 | 3072.77 | 1990.52 |
| 15.99 - 19.99 | 4 | 2.90 | 2.26 | 1.61E-03 | 1.25E-01 | 2.91 | 2.39 | 1059.93 | 825.46 | 0.59 | 45.59 | 1060.52 | 871.05 |
| 0.00 - 5.99 | 10 | 2.25 | 1.55 | 4.61E-03 | 4.98E-03 | 2.25 | 1.56 | 820.22 | 565.79 | 1.68 | 1.82 | 821.90 | 567.61 |
| 5.99 - 15.99 | 10 | 9.66 | 5.88 | 5.93E-03 | 3.66E-02 | 9.67 | 5.92 | 3527.64 | 2145.78 | 2.16 | 13.37 | 3529.80 | 2159.16 |
| 15.99 - 19.99 | 10 | 2.29 | 2.06 | 1.64E-03 | 9.16E-01 | 2.29 | 2.98 | 834.43 | 753.35 | 0.60 | 334.31 | 835.03 | 1087.66 |
| 0.00 - 5.99 | 20 | 4.45 | 2.37 | 3.62E-03 | 5.89E-03 | 4.45 | 2.37 | 1624.73 | 864.22 | 1.32 | 2.15 | 1626.06 | 866.36 |
| 5.99 - 15.99 | 20 | 10.83 | 6.73 | 6.80E-03 | 4.72E-01 | 10.83 | 7.20 | 3951.44 | 2457.07 | 2.48 | 172.38 | 3953.92 | 2629.45 |
| 15.99 - 19.99 | 20 | 3.77 | 2.65 | 1.94E-03 | 7.46E-01 | 3.77 | 3.39 | 1376.76 | 966.84 | 0.71 | 272.19 | 1377.47 | 1239.03 |

Depth-integrated production potentials for each sediment depth increment (shallow: 0 - 5.99 m; intermediate: 5.99 - 15.99 m; deep: 15.99 - 19.99 m). Potential production was calculated for all analytical replicates within a given depth increment, temperature, and headspace treatment, across the final three incubation time points (*n = variable by depth-temperature combination, see* Table 2). For exact calculation of these values please refer to the Methods. Note that rounding differences account for the fact that a few C-$CO_2$ and C-$CH_4$ values do not sum exactly to total carbon values.

nature portfolio

Corresponding author(s): Nancy L Freitas, Margaret S Torn

Last updated by author(s): Oct 25, 2024

# Reporting Summary

Nature Portfolio wishes to improve the reproducibility of the work that we publish. This form provides structure for consistency and transparency in reporting. For further information on Nature Portfolio policies, see our Editorial Policies and the Editorial Policy Checklist.

## Statistics

For all statistical analyses, confirm that the following items are present in the figure legend, table legend, main text, or Methods section.

| n/a | Confirmed | |
|---|---|---|
| ☐ | ☒ | The exact sample size (*n*) for each experimental group/condition, given as a discrete number and unit of measurement |
| ☐ | ☒ | A statement on whether measurements were taken from distinct samples or whether the same sample was measured repeatedly |
| ☐ | ☒ | The statistical test(s) used AND whether they are one- or two-sided<br>*Only common tests should be described solely by name; describe more complex techniques in the Methods section.* |
| ☐ | ☒ | A description of all covariates tested |
| ☐ | ☒ | A description of any assumptions or corrections, such as tests of normality and adjustment for multiple comparisons |
| ☐ | ☒ | A full description of the statistical parameters including central tendency (e.g. means) or other basic estimates (e.g. regression coefficient) AND variation (e.g. standard deviation) or associated estimates of uncertainty (e.g. confidence intervals) |
| ☐ | ☒ | For null hypothesis testing, the test statistic (e.g. *F*, *t*, *r*) with confidence intervals, effect sizes, degrees of freedom and *P* value noted<br>*Give P values as exact values whenever suitable.* |
| ☒ | ☐ | For Bayesian analysis, information on the choice of priors and Markov chain Monte Carlo settings |
| ☒ | ☐ | For hierarchical and complex designs, identification of the appropriate level for tests and full reporting of outcomes |
| ☒ | ☐ | Estimates of effect sizes (e.g. Cohen's *d*, Pearson's *r*), indicating how they were calculated |

*Our web collection on statistics for biologists contains articles on many of the points above.*

## Software and code

Policy information about availability of computer code

| | |
|---|---|
| Data collection | NA |
| Data analysis | All data processing and statistics was done in R (version 4.1.0). The R code used to generate the results of this study is archived and freely available through the ESS-DIVE Repository (DOI: 10.15485/2336866). |

For manuscripts utilizing custom algorithms or software that are central to the research but not yet described in published literature, software must be made available to editors and reviewers. We strongly encourage code deposition in a community repository (e.g. GitHub). See the Nature Portfolio guidelines for submitting code & software for further information.

## Data

Policy information about availability of data

All manuscripts must include a data availability statement. This statement should provide the following information, where applicable:

- Accession codes, unique identifiers, or web links for publicly available datasets
- A description of any restrictions on data availability
- For clinical datasets or third party data, please ensure that the statement adheres to our policy

The data that support the findings of this study are archived and freely available through the ESS-DIVE Repository (DOI: 10.15485/2336866).

## Research involving human participants, their data, or biological material

Policy information about studies with human participants or human data. See also policy information about sex, gender (identity/presentation), and sexual orientation and race, ethnicity and racism.

| | |
|---|---|
| Reporting on sex and gender | NA |
| Reporting on race, ethnicity, or other socially relevant groupings | NA |
| Population characteristics | NA |
| Recruitment | NA |
| Ethics oversight | NA |

Note that full information on the approval of the study protocol must also be provided in the manuscript.

# Field-specific reporting

Please select the one below that is the best fit for your research. If you are not sure, read the appropriate sections before making your selection.

☐ Life sciences ☐ Behavioural & social sciences ☒ Ecological, evolutionary & environmental sciences

For a reference copy of the document with all sections, see nature.com/documents/nr-reporting-summary-flat.pdf

# Ecological, evolutionary & environmental sciences study design

All studies must disclose on these points even when the disclosure is negative.

| | |
|---|---|
| Study description | We incubated a very deep (20-m) sediment core taken below an Arctic lake to constrain the greenhouse gas production from thawed Yedoma permafrost and underlying Quaternary sand and gravel deposits. We provide a critical knowledge advance about greenhouse gas (GHG) production in shallow peats and lacustrine silt-rich mud (0-5 m), intermediate thawed Yedoma silt (6-15 m), and deep unconsolidated fluvial sediments (16-20 m). We address three existing gaps in understanding within permafrost research: 1) how the geochemistry of a thaw bulb varies along a deep sediment profile; 2) which sediments contribute to the highest GHG production; and 3) how microbial carbon dioxide (CO2) and methane (CH4) production changes across depth, redox, and climate warming scenarios.<br><br>We conducted 365-day incubations, radiocarbon-dated select organic materials, and classified depth increments. Briefly, parallel aerobic and anaerobic sediment incubations were run at three temperature treatments (4°C, 10°C, 20°C); all depths were incubated at 4°C and five depths were also incubated at 10°C and 20°C. Each oxygen-temperature-depth combination was incubated in triplicate. Measured values were used to calculate cumulative greenhouse production in terms of total carbon released, global warming impact of carbon released (C-CO2e), and temperature sensitivity across depths and time periods (Q10). |
| Research sample | Sediment coring was conducted March 16-17, 2018 in the north-central basin of Goldstream Lake (GSL, 64.916°N, 147.847°W) at a water depth of 1.39 m. All samples were collected (and exported) in a responsible manner and in accordance with relevant permits and local laws. GSL is a thermokarst lake formed in Yedoma permafrost and located in the Goldstream Valley in interior Alaska, ~15 km north of Fairbanks. GSL was selected because it is well studied with respect to methane emissions and thaw bulb (talik) properties, though very little work has been done on lake sediments and none on the deep talik sediments. The region is characterized by discontinuous permafrost. |
| Sampling strategy | A vibracorer was used to extract surface sediments (down to 4.40 m) in a single core tube (64.91588°N, 147.84901°W ± 9 ft). In an immediately adjacent coring site (64.91582°N, 147.84935°W ± 9 ft), a Boart Longyear diamond core drilling system was used to extract deeper sediments (down to 20.13 m) using percussion drilling. The coring setup consisted of a casing around the borehole that extended up through the lake water and ice to just below the drill rig. A core barrel with a plastic liner inside traveled up and down inside the casing. The casing was not installed at once down to 20 m; it was pushed down in 3.2 m sections incrementally as the coring progressed. Continuous core sections were extracted in clear plastic liners (8.9 cm ID) nested in a 1.8 m long core barrel from within the cased sediments. No intact permafrost was encountered during coring.<br><br>For laboratory incubations, 150-200 g of sediment was taken from 35 selected core depths. At each sampling location, sediment was collected between two points that spanned 14-16 cm of vertical core depth. Parallel aerobic and anaerobic incubations were then conducted on 12 of the 35 sample depths collected from the core. The 12 depths provided as much vertical coverage of the sediment as possible (given the quantity of sediment available for processing replicates and treatment conditions), and spanned the different paleoconditions of the core (based on sediment depth classifications and 14C sampling sites). |
| Data collection | For incubations -- at each sampling time point, 7 mL of gas was collected from the headspace of every bottle using a syringe. The volume of gas pulled from each incubation bottle was replaced by an equal amount of either C-free air or N2 to maintain appropriate oxic / anoxic conditions for microbial communities and to keep serum bottle pressure at equilibrium. Raw CO2 and CH4 concentrations at each sampling time point were determined by GC analysis throughout the incubations. Every gas sample taken |

| | |
|---|---|
| | from a bottle represented the accumulated amount of CO2 and CH4 respired up until that day, diluted by 7 mL per time point since the beginning of the incubations. Author NLF led the data collection and sampling with assistance from author RCP. |
| Timing and spatial scale | Incubation bottles were sampled with high frequency at the beginning of the incubations to capture the initial respiration responses (twice per week for the first month), and were gradually scaled down to a lower sampling frequency near the end of the incubations as production rates stabilized (once per month for the final five months). Spatially, the core represents one of the longest sediment cores ever taken from below an Arctic lake - it provides more sediment vertical coverage for incubations studies than nearly all recent permafrost lake literature. |
| Data exclusions | Four time points were dropped from aerobic and anaerobic CO2 data (days 99-117, and days 167-223, respectively), as they were deemed implausible due to negative fluxes. We did not use these data and assumed zero respiration at those time points. |
| Reproducibility | All methods associated with this study are rigorously reported in the Methods section of our manuscript, and the code was written in a manner to encourage use by other scientists conducting similar studies. Given that conducting deep sediment coring is highly resource intensive (personnel, equipment, finances, etc.), we report novel data on one core that was able to be obtained at a 20-m depth. |
| Randomization | For sediment characterizations -- cut-off syringes were used to obtain 5 mL sediment plugs at 150 depths for analysis of percent moisture, bulk density, magnetic susceptibility, macrofossils, total nitrogen (Ntot), total C (Ctot), total organic C (Corg), total inorganic C (Cinorg), 14C dating, and δ13C. Sediment plugs were taken at a sampling frequency of 5-10 cm from the shallow cores, and approximately every 10-20 cm from the deep cores.<br><br>For incubations -- at each sampling location along the core, sediment was collected between two points that spanned 14-16 cm of vertical core depth. Sediment for incubation jars was subsampled randomly across the available material to capture the heterogeneity of the 14-16 cm of core depth in each sample bag. |
| Blinding | Blind analysis was not possible during this study as it was necessary to know which sediment depths respired a given quantity and type of carbon gas. This is because we needed to flush specific jars if they reached too high of greenhouse gas concentrations so as not to jeopardize the study. |

Did the study involve field work? ☒ Yes ☐ No

## Field work, collection and transport

| | |
|---|---|
| Field conditions | Goldstream Lake (GSL; .010 km2, 4.4-m maximum depth) formed from the melting of permafrost ground ice in late Pleistocene Yedoma-type deposits. Pooled water thawed previously frozen Quaternary aeolian deposits both vertically and laterally, allowing for sediment thaw (thermokarst) expansion at depth and along lake margins. A partial drainage event occurred between 1949 and 1978, but GSL is still undergoing active thermokarst expansion along its eastern and southern edges. Extensive studies have been conducted on GSL that describe ebullition (bubbling) and diffusive GHG composition, distribution, and flux. Physical and chemical analyses have also been conducted on the surface water and surface sediments of the lake.<br><br>GSL is located in the Goldstream Valley in interior Alaska, ~15 km north of Fairbanks. It was selected because it is well studied with respect to methane emissions and talik properties, though very little work has been done on lake sediments and none on the deep talik sediments. The region is characterized by discontinuous permafrost. Annual atmospheric temperature and precipitation averages are -2.4°C and 274 mm, respectively (Fairbanks International Airport, 1981–2010 Annual/Seasonal Normals, U.S. National Climatic Data Center). |
| Location | Sediment coring was conducted March 16-17, 2018 in the north-central basin of GSL at a water depth of 1.39 m. The coring location represented the approximate center of the lake in 1949. A vibracorer was used to extract surface sediments (down to 4.40 m) in a single core tube (64.91588°N, 147.84901°W ± 9 ft). In an immediately adjacent coring site (64.91582°N, 147.84935°W ± 9 ft), a Boart Longyear diamond core drilling system was used to extract deeper sediments (down to 20.13 m) using percussion drilling. |
| Access & import/export | All relevant permits and permissions were acquired by author KWA at UAF in preparation for sediment coring in 2018, in adherence with protocols established under grant NSF P2C2 1903735. All samples were collected (and exported) in a responsible manner and in accordance with relevant permits and local laws. |
| Disturbance | Disturbance was minimized by utilizing appropriate field technique for all fieldwork, only extracting cores from two locations in the lake center, and only removing sediment from the lake that was relevant to the study. |

# Reporting for specific materials, systems and methods

We require information from authors about some types of materials, experimental systems and methods used in many studies. Here, indicate whether each material, system or method listed is relevant to your study. If you are not sure if a list item applies to your research, read the appropriate section before selecting a response.

## Materials & experimental systems

| n/a | Involved in the study |
|---|---|
| ☒ | ☐ Antibodies |
| ☒ | ☐ Eukaryotic cell lines |
| ☒ | ☐ Palaeontology and archaeology |
| ☒ | ☐ Animals and other organisms |
| ☒ | ☐ Clinical data |
| ☒ | ☐ Dual use research of concern |
| ☒ | ☐ Plants |

## Methods

| n/a | Involved in the study |
|---|---|
| ☒ | ☐ ChIP-seq |
| ☒ | ☐ Flow cytometry |
| ☒ | ☐ MRI-based neuroimaging |

# Plants

| | |
|---|---|
| Seed stocks | NA |
| Novel plant genotypes | NA |
| Authentication | NA |